THEORETICAL AND EXPERIMENTAL INVESTIGATIONS ON TYPICAL BLADES IN CASCADES

By
Y. V. L. N. MURTHY

DEPARTMENT OF AERONAUTICAL ENGINEERING
INDIAN INSTITUTE OF TECHNOLOGY KANPUR

AUGUST 1973

THEORETICAL AND EXPERIMENTAL INVESTIGATIONS ON TYPICAL BLADES IN CASCADES

A Thesis Submitted
In Partial Fulfilment of the Requirements
for the Degree of
MASTER OF TECHNOLOGY

By
Y. V. L. N. MURTHY

to the

DEPARTMENT OF AERONAUTICAL ENGINEERING
INDIAN INSTITUTE OF TECHNOLOGY KANPUR

AUGUST 1973

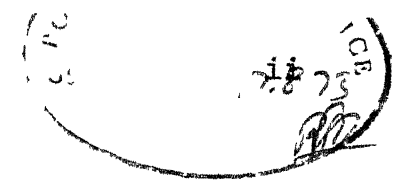

CERTIFICATE

Certified that this work "THEORETICAL AND EXPERIMENTAL INVESTIGATIONS ON TYPICAL BLADES IN CASCADES has been carried out under my supervision and that the work has not been submitted elsewhere for a degree.

(C.S. Moorthy)
Associate Professor
Department of Aeronautical Engineer
Indian Institute of Technology, Kan

31.8.73

ACKNOWLEDGEMENT

The author desires to express his deep sense of gratitude to Prof. C.S. Moorthy and gratefully acknowledge the guidance and encouragement given by him.

The author is grateful to the Hindustan Aeronautics Limited for sponsoring to the second year of the M.Tech. programme.

The author desires to express his thanks to Shri R. Krishna Murthy for his help in the fabrication part. Thanks are due to Mr. C.V.C. Rao for helping in running the Computer Programmes. Thanks are due to Mr. G.L. Narasaiah for helping in arranging the work.

Thanks, too, are given to Mr. S.Kumar for fine typing, to Mr. P.K. Malhotra for nice drawings.

CONTENTS

LIST OF SYMBOLS

P_o	total pressure
p	static pressure
W	velocity
ΔP_o	total pressure loss
β	air angle
C_p	pressure coefficient
R_e	Reynolds number based on chord
t	pitch length
L	chord length
ζ_v	profile loss coefficient
ζ_T	total loss coefficient
λ	stagger angle
AVR	axial velocity ratio

SUBSCRIPTS

1	far upstream
2	far downstream
y	tangential direction
z	axial direction
t.e.	trailing edge
l.e.	leading edge
k	local point along the chord
TH.	theoretical
EXP.	experimental

ABSTRACT

Experiments are conducted on cascades of four differ
ent types of blade sections, viz., one compressor and three
turbine blade sections at various inlet angles, under unifo
upstream and downstream conditions. For each setting of the
solidity, stagger and inlet angle, the surface pressures
are tapped and a survey is made at half-chord downstream
to the trailing edge, to obtain the downstream flow conditi
Stall limits are established and the optimum operating
conditions are selected based on a compromise between the l
and the deflection in all possible cases.

Boundary layer measurements are taken at the traili
edge plane, to obtain the profile losses, in the case of
unseparated flows. In the case of separated flows the point
of separation is located approximately and the freestream
velocity corresponding to the separation point is measured.

In all the cases, corresponding to zero incidence,
theoretical calculations are made for the 2-D potential flo
velocity distributions and profile loss coefficients. The
theoretical results are compared with the experimental val

CHAPTER I

INTRODUCTION

In an axial flow turbomachine, if the blades are relatively short in the radial direction, the change in the radius of a particle passing through a blade row can be assumed to be small. If the blades are bounded by the cylindrical walls, the cylindrical flow thus can be studied by stretching the row of blades into an infinite plane, known as the cascade of airfoils. Hence, the theoretical calculations and experimental correlations made on such cascades can be used in the design calculations of the turbomachines with reasonable accuracy, though the complexity of the actu 3-D flow is not solved. A number of theoretical methods wer developed besides experimental techniques to obtain perfect correlations between the geometric parameters and the aero mic parameters.

Results of the earlier tests on cascades with solid side-walls were not satisfactory and varied from tunnel-to- tunnel. The growth of the boundary-layer along the solid s walls and its interaction with the blade boundary-layer in duced 3-D effects. Experiments were conducted to determine the influence of the aspect ratio, boundary-layer control by means of slots and porous surfaces and tunnel end wall

calculations upon the airfoils in cascades. It was concluded that the disparity from the 2-D calculations was comparatively lesser in the case of turbine cascades when the tests were conducted at aspect ratios > 3. |1|. Numerous tests were conducted by various workers; performance curves in the form of section characteristics and pressure distributions were plotted varying the cascade settings and the inlet flow-conditions. |2, 3, 4, 5|. The results were compared with the available theory and the test techniques were thus gradually improved.

A number of methods had been proposed to obtain the theoretical flow through cascades of airfoils (direct problem) or to obtain a desirable airfoil shape (inverse problem) for the blade sections; including analytical methods using conformal mapping |6, 7|, graphical procedures |8|, singularity methods due to Schlichting |9| and other analogues, viz. Mechanical and Electrical |10|. A simple unified approach to the direct and inverse problems of compressible flow past cascades was presented by Chung-Hua and Courtis A. Brown |11|.

Viscosity effects on the 2-D cascade were studied to analyse the 2-D losses which were explained to be due to the formation of boundary-layers on the airfoil surfaces. Many theories had been put forward to calculate losses solving Von-Karmann's integral equation, for both laminar and turbulent

flows. [12, 13, 14], The velocity distribution obtained by potential flow theory was the starting point for all these methods to estimate losses.

The aims of the present work are as follows:

(a) to obtain uniform upstream and downstream conditions at all angles of attack covering the region between the stall limits,

(b) to obtain the surface pressure distributions along the chord for various configurations and to compare the pressure distributions at 'zero' incidence with those obtained theoretically,

(c) to set-up stall limits and optimum operating conditions for all possible cases by drawing the deflection vs. losses, characteristic curves,

(d) to measure the boundary layers at the trailing edge (for unseparated cases only) for the purpose of obtaining the profile losses and to compare with the losses at half-chord downstream,

(e) to calculate the profile losses using the available theory to compare with those obtained experimentally.

The tests are conducted on the available cascades of blades using the cascade tunnel of the Department of Aeronautical Engineering. All the tests are conducted with solid end walls and at the aspect ratio of 3. The potential flow

velocity distributions are obtained by the channel flow technique outlined in Ref. |11|. Profile losses, for both separated and unseparated flows, are calculated using boundary layer theory outlined in Ref. |12, 13, 14|.

CHAPTER 2

EXPERIMENTAL WORK

2.1 General:

The cascade tunnel of the department, fitted with the test section of 15" x 12" cross-section is used for the present experimentation. The wind tunnel is driven by a 30 hp. constant speed motor and the shutter arrangement near the eye of the tunnel provides for the control of the air speed ranging from a minimum of 20 ft./sec. to a maximum of 145 ft./sec. at 25°C and 28.04" of mercury.

2.2 Details of Models and Test Section:

The series of tests was made on cascades with five blades. The cascade blades were fabricated from the seasoned wood and were given a shellac finish. The profiles were of four inch chord and were shaped using templates. Pressure instrumentation was provided on the surface of the blades by burying hyperdermic tubing just below the surface and drilling static holes through at the central position.

The test section was made of plywood with a finished inner surface. Adjustable side vanes were fitted on to the sides of the test section and tufts were fixed on the blade surfaces at regular intervals. The position of the side vanes

relative to the end airfoils in cascade was determined such that the effect of the side vanes on the pressure distribution over the central airfoil was the least. The aluminium plates of 17" ϕ were turned and were positioned on the upper and lower surfaces of the test section. The blades were fixed between the plates and the angle of attack of the upstream was set by rotating the upper disc. The stagger was set by rotating the blade through the required angle about the pivotal point fixed at the leading edge. All the tests were conducted at a constant aspect ratio of three and Reynolds numbers (based on blade chord and upstream dynamic head) ranging from 2.5×10^5 to 3.0×10^5.

2.3 Instrumentation:

2.3.1 Upstream measurements:

Fine static holes were driven on the upper disc at a distance of one chord length upstream to the line of leading edges, (Ref. 16) the uniform reading given by which was taken as the upstream static head. The inlet angle measuring arrangement consisting of an yaw probe and a protractor, was fitted on the upper disc along the central line of the disc at a distance of half chord length upstream to the line of leading edges. A pitot-tube, for the upstream stagnation pressure measurement, was fitted on to the tunnel side wall. The static

and stagnation readings were comparable with the readings obtained by the standard pitot-static tube within ± 2%. The sensitivity of the yaw probe is ± 0.1 units per 1° variation, the unit being $(\Delta_{pl}/q_{1\infty})$; Δ_{pl} = difference in the levels of the U-tube manometer limbs and $q_{1\infty}$ = the upstream dynamic head.

2.3.2 Downstream measurements:

A combination probe (Fig.2) was fitted for measuring the stagnation pressure, static pressure and the outlet angle at the same point simultaneously. (Ref. 15). The readings of the static and stagnation pressure tubes departed from the readings of the standard pitot-static tube only by ± 1.5%. The sensitivity of the yaw probe is ± 0.1 units per 1.5° change. The combination probe together with the protractor was mounted on the traverse which in turn was fitted on the upper disc at 1/2 chord length downstream of the line of the trailing edges. (Ref. 16).

2.3.3 Boundary-layer probes:

In the cases of unseparated flows the boundary layer survey was made in the plane of trailing edges on the central airfoil. The boundary-layer probe (Fig.3) was used for this purpose. The static pressure was measured at 1/2" below the

points where the stagnation pressure was measured, after confirming that the difference between the static pressure at the central plane and at the plane 1/2" below to that was minimum. The stagnation and static pressure readings were accurate within ± 2% relative to the standard pitot-static tube readings.

In the case of the separated flows it was necessary to locate the point of separation. A pitot tube (Fig.4) was used for the approximate location of the point of separation.

A traversing gear fitted with the micrometer (least count 0.001") was fixed to a plummer block which in turn was mounted on the upper aluminium disc. The boundary layer probe was fitted to the traversing arrangement through rigid connections so as to avoid any possible displacement of the probe from its position due to the turbulence in the stream.

Readings across the boundary-layer were taken using a projection manometer of a magnification ratio 10:1. Multi-tube manometers were used for measuring the static pressures on the airfoil surface and the yaw probe leads were connected to the limbs of the 'U' - tube.

2.4 Experimental Procedure

Before making any measurements, the checks that were made include, (1) the uniformity of the flow in the tunnel at

various planes, viz., 3", 6" and 9" from the upper surface; (2a) the uniformity of upstream static pressure readings, (2b) the uniformity of the downstream readings across each channel, (to achieve the above mentioned uniform conditions the end vanes were adjusted for each inlet angle set-up) and (3) any possible warping of the airfoils (checked using templates).

The upstream angle of attack was set by the upstream yaw probe and the disc was rotated until the manometer limbs showed equal reading approximately. The positions of the side vanes were adjusted until uniform conditions were achieved in the upstream and downstream and then the angle of attack was set exactly. The upstream static and stagnation heads were read. Blade pressure distribution was measured at the mid-span position of the central airfoil at each angle of attack. Survey of the total pressure, outlet angle and static pressure were made at a distance of 1/2 chord length downstream to the line of leading edges. All the downstream measurements were made at 0.5" intervals across the pitch of the central airfoil and were averaged to obtain the final value.

Boundary-layer survey for the unseparated flows was made in an axial plane at a distance 0.95% chord length from the line of leading edges. In the case of the separated

flow, the pitot-cube was traversed along the chord for the required gradient characterising the point of separation. The freestream velocity head at the point of separation was obtained from the static pressure distribution curve coupled with the freestream stagnation reading.

2.5 Data Reduction:

1.a) Pressure coefficient (turbine blade)

$$C_{pt} = \frac{p-p_2}{1/2\ W_2^2}$$

b) Pressure coefficient (compressor blade)

$$C_{pc} = \frac{p-p_1}{1/2\ W_1^2}$$

2. Loss coefficient

$$\bar{\omega}_T = \frac{P_{o1} - P_{o2}}{1/2\ W_a^2}$$

3. Coefficient for Ackerets criterion for stall:

$$\alpha = \frac{p_{t.e.} - p_{min.}}{p_o - p_{min.}}$$

stall at $\alpha = 0.7$ and onwards.

$p_{min.}$: the minimum static pressure along the blade.

4. Contraction coefficient, C_c

$$C_c = \frac{W_2 \cos \beta_2}{W_1 \cos \beta_1} - 1$$

CHAPTER 3

THEORETICAL WORK

3.1 Potential Flow Calculations

The theoretical analysis of the potential flow in 2-dimensions through cascades of airfoils concerns with two problems, viz., (1) the direct problem and (2) the inverse problem. In the direct problem the geometry of the cascade and a characteristic velocity are given and the velocity are given and the velocity distribution on the surfaces is obtained. In the inverse problem the velocity distribution on the surfaces along with the upstream and downstream velocities is given and the corresponding geometry of the blade is obtained.

Many methods are available for the solutions of both the problems depending upon the order of solidity, whether low or high. Transformation methods developed in Ref. |6| are more laborious and time consuming because of the number of transformationsinvolved. Hodograph techniques suggested in Ref. |7| can be computarised but the accuracy is found to be limited to solidities less than 1.0. The singularity distribution methods due to H. Schlichting are suitable for thin airfoils with a small camber. The proposed analogies (10) give a qualitative picture of the flow, but

are not readily useful for the design of the blade surfaces. The relaxation methods [10] are time consuming in view that the initial approximations may not be nearer to the correct values. The method suggested by Ref. [11] provides a solution for the direct and inverse problems, which is accurate enough in the case of incompressible flow and can be a starting value for the relaxation method to obtain a more accurate solution in the case of a compressible flow. In the present work, method of Ref.[11] is used to solve the direct problem for four types of blades in cascade.

3.1.2 Details of the method:

Calculation is made for the flow along a particular stream line (reference line) in the channel, formed by two neighbouring blades. To start with the mean stream line, which is obtained by taking the mean of the upper and lower surface coordinates of the blade in the tangential direction, is taken as the reference line. From the given channel width distribution along the axial-direction, the velocity distribution along the line of reference is computed using the continuity and the two-dimensionality considerations. Partial derivatives along the tangential direction are obtained using the equations of motion and continuity. Streamlines are set-up on either side of the reference line using the Taylor series

and the final streamline thus obtained on either side of the reference line matches with the given suction and pressure surfaces. In the case of any disparity between the final streamline and the surface beyond the specified limit, the position and/or the shape of the mean stream line is corrected.

3.1.3 Assumptions made:

1. Flow is two-dimensional, incompressible and non-viscous.
2. The axial velocity on the reference line closely follows the channel width ratio.
3. The shape of the reference line closely follows the blade mean line.
4. Kutta condition is neglected in view to be more nearer to the real flow conditions. (because of the t.e. thickness.)

3.1.4 Fixing the inlet and exit angles:

It is observed that any changes in the shape of the reference line at the entrance and exit to the channel are carried over to the central points thus effecting the flow calculations. As the comparisons are made with the experimental values, the inlet and exit line shapes are fixed as per the measured directions of the flow. In all the cases the inlet flow directions correspond to the zero incidence, because it is at this angle of attack, the effects of induced flow are negligible, thus the difference between the measured flow direction (at a distance of one chord length upstream to the line of leading

edges) and the actual flow direction (right at the plane of the leading edges.) is less.

3.1.5 Difficulties encountered:

1. In some cases, it is found that the subsequent streamlines obtained are not uniform, thus the further streamlines obtained are erroneous. In such cases the streamlines are smoothened using polynomial regression of the order two.

2. When the initial reference line is far from the actual line (dividing the mass flow into two halves) the divergence is found to take place. In such cases a manual correction to the shape of and flow on the mean line is made.

3.1.6 Mathematical relations:

The tangential velocity, $W_y = W_z \tan \beta$ where $\tan \beta$ is the slope of the streamline (2-D considerations).

The successive terms of the Taylor series include the partial derivatives for extending the flow from the reference line. The details are given in Appendix 'A'.

$$\frac{\partial W_z}{\partial y} = \left(\frac{dW_y}{dz} + \frac{dW_z}{dz} \tan \beta\right) \cos^2 \beta$$

$$\frac{\partial W_y}{\partial y} = \left(\frac{dW_y}{dz} \tan \beta - \frac{dW_z}{dz}\right) \cos^2 \beta$$

and the other derivatives of other orders follow. The total derivatives are calculated numerically using the central difference formulae. All the velocity terms are non-dimensionalised with respect to the axial velocity at the entrance far off, and all the length terms are non-dimensionalised with respect to the axial chord.

The successive streamlines are obtained from the consideration of equal mass flow through each channel formed by two adjacent streamlines. Mass flow between streamline 1 and reference line is given by,

$$M/8 = W_{z1}\, t/8\, h = \int_{\text{ref.}}^{1} W_z\, h\, dy$$

h : blade height

W_{z1} : axial velocity at the entrance

M : total mass flow

using the non-dimensional quantities,

$$1/8\ t/L = \int_{\text{ref.}}^{1} \frac{W_z}{W_{zi}}\, d\,(y/L)$$

Knowing W_z at any 'y' from the Taylor's series expansion we can get either the mass flow between two fixed streamlines or the coordinates for the required mass flow.

In the present calculations only the first two terms of the series are taken for calculating the flow on the

succeeding streamlines. The pressure coefficient is calculated on the basis of exit angle for turbine cascades and on the basis of inlet angle for the compressor cascades. The results are presented in the form of graphs (comparisons) and tables.

3.2 Loss Calculations:

3.2.1 General:

In a real flow through 2-D cascades boundary-layers develop both on the suction and pressure surfaces of the air-foils and form blade wake after leaving the trailing edge. As the wake moves downstream, a mixing takes place between the wake and the free stream and through viscous action the flow becomes uniform at some distance behind the trailing edge. The 2-D losses are explained to be due to the formation of these boundary layers.

The theoretical calculations of losses can be expressed in 2 stages, viz., (1) calculations of the potential flow pressure distributions on the blade surfaces and (2) calculation of the boundary layer parameters solving the integral equation by approximate theories using the above pressure distributions.

3.2.2 Assumptions:

(1) Boundary-layer is completely turbulent.

(2) So far as the separation does not occur, the

potential flow pressure distribution closely follows the actual pressure distribution.

3.2.3 Formulae used:

The formula for the approximate calculation of the turbulent boundary-layer is due to (E.Truckenbrodt) - given in Ref. |14|.

$$\frac{\theta_H}{L} = \left(\frac{\bar{W}}{W_{t.e.}}\right)^3 \left[\left(\frac{C_f}{2}\right)^{\frac{n+1}{n}} \int_0^1 \left(\frac{W_k}{\bar{W}}\right)^{3+\frac{2}{n}} d\left(\frac{k}{L}\right)\right]^{n/n+1}$$

θ_H : momentum thickness at the trailing edge.

$\bar{W}$: chosen reference velocity (downstream experimental value)

$W_{t.e.}$: velocity at the trailing edge.

W_k : velocity distribution on the blade surface along the axial-direction

C_f = frictional coefficient,

$= 0.074\ R_e^{-1/1+n}$

and $n = 4$ for $R_e = 10^5$ to 10^7.

The loss coefficient is defined as,

$$\zeta_v = \frac{P_{ot.e.}}{1/2\ W_z^2}$$

$P_{ot.e.}$ = total pressure defect at the trailing edge.

From Appendix 'B' the value of ζ_v can be shown as,

$$\zeta_v = \frac{2\theta}{t \cos^3 \beta_2}$$

where θ : total momentum thickness at the trailing edge.
In the present calculations β_2 is taken as the outlet angle measured downstream.

The method can be extended to separated flows also, provided that the separation has taken place in the regions nearer to the trailing edge. An additional momentum thickness, θ_{sep} due to separation, is to be added to the total momentum thickness, 'θ' at the trailing edge,

$$\theta_{sep} = 1/2\ y_{dA} \left[\left(\frac{W_A}{W_{t.e.}}\right)^2 - 0.9 \right] \text{ (Ref.12)}$$

y_{dA} : half-profile thickness at the separation point.

W_A : freestream velocity at the separation point.

$W_{t.e.}$: velocity at the trailing edge.

The boundary-layer profiles obtained by a survey at the trailing edge are presented for both suction and pressure surfaces. The values of calculated and measured loss coefficien are plotted for the matching purposes.

CHAPTER 4

RESULTS AND DISCUSSIONS

The effect of end vanes position relative to the end blades on the pressure distribution over the central blade of the cascade is shown in Fig.5. It is observed that the effect is less as the gap between the end vanes andthe end blades is more than 0.8 pitch length, in the case of the turbine blade root c/s at $\beta_1 = 45^\circ$ and $\lambda = +15^\circ$; with uniform downstream readings. Similar investigations on the other sets of blades for various configurations revealed that the minimum gap should be more than 0.8 pitch length. In the experimentation, the gap was fixed to be of one pitch length for the turbine blades and 0.8 pitch length for the compressor blades.

Fig. 6 sets a limit on the ratio of $(\text{Cos } \beta_1/\text{Cos } \beta_2)$ for various configurations regarding the validity of the data. For a contraction coefficient less than 0.08 the limiting ratios are as under:

Blade No. 4 (see Appendix 'C')

(a) $\lambda = 0^\circ$ t/L = 2.5/4.0 ratio = 0.88

(b) $\lambda = -5^\circ$ t/L = 2.5/4.0 ratio = 0.86

(c) $\lambda = -15^\circ$ t/L = 3.0/4.0 ratio = 0.60

The ratios corresponding to the configurations $\lambda = 0^{\circ}$ and -5° with t/L = 3.0/4.0, varied little from the ratios of configurations $\lambda = 0^{\circ}$ and -5° with t/L = 2.5/4.0 respectively. In general, there is an increase in the contraction coefficient at high incidences and at regions near positive stall the contraction coefficients are beyond the plot dimensions.

Similar curves in Fig. 7 set limits on ($\cos \beta_2 / \cos \beta_1$) ratios for turbine blade sections. For a contraction ratio of 0.20 the limiting ratios are as under:

(a) blade no. 1 $\lambda = 15^{\circ}$ t/L = 3.0/4.0 ratio = 1.0

(b) blade no. 2 $\lambda = 15^{\circ}$ t/L = 3.0/4.0 ratio = 1.0

(c) blade no. 3 $\lambda = 15^{\circ}$ t/L = 3.0/4.0 ratio = 0.98

For the remaining configurations with the turbine blade sections the contraction coefficients exceed 0.20. In general the contraction coefficient increases with incidence for turbine blade cascades also.

Thus as seen from Figs. 6 and 7 the extent of two-dimensionality conditions attained in the tunnel test section for the compressor and turbine blade sections are upto 0.08 contraction coefficient and 0.20 contraction coefficient respectively.

In Figs. 8 to 11, stall limits are set up based on useful operating range in all the cases. For the turbine blade sections at stagger angles lower than + 15°, no useful range of operation is found, indicating that the blades stalled at all the angles of attack. In the case of the compressor blade sections significant operating range is found for all the stagger angles, viz., 0°, -5° and -15°; though the range is not wider at -15° stagger comparatively.

The effect of solidity variation from 4/2.5 to 4/3 is not significant either on the losses or on the useful operating range (Fig.8). Inlet angles corresponding to the stall limits can be obtained from Figs. 12 to 15 knowing the deflections from Figs. 8 to 11. Arrow marks in Figs. 8 to 15 correspond to the stall limits.

Satisfactory agreement of the theoretical and experimental pressure distributions corresponding to zero incidence is observed in the case of the blade no.4 at staggers of 0° and -5° with t/L ratio of 2.5/4.0 and 3.0/4.0; and in the case of the blades 1, 2 and 3 at $\lambda = 15^{\circ}$ with t/L ratio of 3.0/4.0, within the margin of experimental errors and the assumptions upon which the theory is based (Figs. 16 to 18). The disparity is found to be in the other cases and the reasons may be that;

(a) at low stagger angles, in the present blade configurations, the A.V.R. across the turbine cascade is far

from unity, and hence the flow is no longer 2-dimensional.

(b) In the theoretical calculations the axial-velocity is taken to be the mean value of the upstream and downstream values, though the AVR is very high in the case of the turbine blades at low stagger angles,

(c) with the decrease in the stagger angle local separation of the flow has taken place in the divergent sector of the convex surface.

In general, it is noted that the area of the theoretical loop is greater than the area of the experimental loop. This implies that theoretical lift coefficient is greater than the experimental lift coefficient.

The effects of stall on the surface pressure distribution can be observed from Fig. 19. The flattening of the pressure distribution curve, corresponding to the stalled position, in the regions of the trailing edge indicates that the flow has separated near the region of the trailing edge.

Boundary layer profiles, as measured at 0.95 chord of the blade section are represented in Figs. 20 to 22. The profiles obtained on the concave surface are found to be more compact than the profiles on the convex surface. This may be because of the fact that over the concave surface the flow near the trailing edge is always convergent. The profiles on

the concave surface are found to follow the equation,

$$\frac{W}{W_\delta} = (y/\delta)^{1/n}$$

with the value of n between 2.5 to 3.0.

δ = boundary layer thickness

Momentum thickness on the concave surface is about 1/3 to 1/5 of the momentum thickness on the convex surface (Tables 21 and 22). Hence, the main influence of the dependence of the profile losses will be exerted by the losses on the convex surface of the profile.

Profile losses, calculated, based on the boundary layer curves obtained at the trailing edge are compared with the theoretical calculations in Fig. 24. The profile losses are found to be about half the total loss coefficients, obtained from the downstream survey, indicating that the mixing and secondary losses together are approximately of equal magnitude to the profile losses (Tables 21 and 22).

The results of the direct problem are shown in Figs. 25 to 34. In general, the following points are noted:

(a) the mean-stream line is away from the blade-mean-line towards the suction surface,

(b) the error in the calculations is large on the suction surface,

(c) the error in the calculations increased as the solidity decreased,

(d) the error in the calculations is large at the edges.

Conclusions

1. Uniform conditions are disturbed as the angle of attack increased.

2. In general the area of the theoretical pressure distribution curve is greater than the area of the experimental pressure distribution curve.

3. The useful operating range increased with the increase of stagger in the case of turbine blades and increased with the decrease of stagger in the case of compressor blades.

4. The losses at half-chord downstream are found to be about twice the losses at the trailing edge.

5. The losses on the suction surface are 3 to 5 times larger than the losses on the pressure surface.

SUGGESTIONS FOR FURTHER WORK

A better agreement between the theory and experiment can be achieved by adopting boundary layer control on the side walls and in the theoretical point of view, by recalculating the velocities using relaxation techniques taking into consideration the compressibility effects also. The present values can be taken as starting values for the relaxation techniques.

An iterative scheme may be developed, to obtain better theoretical predictions, considering the circulation defect. (In the present work it is seen that the theoretical lift coefficient is greater than the experimental value.)

Experiments may be conducted for various combinations of Reynolds numbers, mach numbers and upstream turbulence levels.

Experiments may be conducted to measure the induced angle, so as to obtain the actual angle of attack as against the angle of attack obtained by the yaw probe.

With the above modifications both in the theory and experimentation a number of blade sections can be studied at various configurations and correlations can be established between the aerodynamic parameters and the geometric parameters of the cascades.

REFERENCES

1. John R. Erwin and Jones C. Emery, 'Effect of Tunnel Configuration and Testing Technique on Cascade Performance', NACA TN 2028, 1950.

2. S.Katzoff and Margery E. Hannah, 'Further Comparisons of Theoretical and Experimental Lift and Pressure Distributions on Airfoils in Cascades at Low Subsonic Speeds', NACA TN 2391, 1951.

3. James C. Dunavant and John R. Erwin, 'Investigations of a Related Series of Turbine-blade Profiles in Cascades', NACA TN 3802, 1956.

4. John R. Erwin, Melryn Savage and James C. Emery, '2-D Low-speed Cascade Investigations of NACA Compressor Blade Sections Having a Systematic Variation in the Mean-line Loading', NACA TN 3817, 1957.

5. Joseph Herrig, John C. Emery and John R. Erwin, 'Systematic 2-D Cascade Tests on NACA 65-Series Compressor Blades at Low Speeds', NACA TN 3916.

6. Howell, A.R., 'Theory of Arbitrary Airfoils in Cascades', Phil. Mag. Ser. 7.39913 (1941).

7. H.N. Cantrell and J.E. Fowler, 'The Aerodynamic Design of 2-D Turbine Cascade for Incompressible Flow with a High Speed Computer', J. of Basic Engg., 1959, pp. 349-361.

8. Stodola, 'Steam and Gas Turbines', Vol. II, pp.992-994 and 998-1006.

9. G.T. Csanady, 'Theory of Turbomachines', pp. 222 to 229.

10. William H. Rowdebush, 'Potential Flow in 2-D Cascades', pp. 101 to 149, NACA SP-36, 1965.

11. Chung-Hua and Curtis A. Brown, 'A Theory of Direct and Inverse Problems of Compressible Flow Past Cascades of Arbitrary Airfoils', J. of Aero.Science 19, 1952, pp. 183-196.

12. Herrmann Schlichting, 'Application of Boundary-layer Theory to Turbomachines', J. of Basic Engg. D 81, pp. 543-552, 1957.

13. Charles A. Mac. Gregor, '2-D Losses in Turbine Cascades', J. of Aero. Science, Vol. 19, 1952.

14. 'English Electric', Library Translations-1031.

15. W.R. Hawthrone, 'Aerodynamics of Turbines and Compressors', Vol. X, High Speed Aerodynamics and Jet Propulsion, Chapter: D,3. Instrumentation, pp. 192 to

195, Princeton University Press, 1964.

16. W.R. Hawthrone, 'Aerodynamics of Turbines and Compressors', Vol. X High Speed Aerodynamics and Jet Propulsion, Chapter: D, 4 2-D Cascades, pp. 218 to 232, Princeton University Press, 1964.

17. A. Charwat, 'Note on Two-dimensional Losses in Cascades', 19, J. of Aero. Science-Reader's Form, 1952, pp. 851-852.

APPENDIX 'A' (Ref. [11])

The steady 2-D flow of a non-viscous incompressible fluid is governed by the following equations of continuity and irrotationality:

$$\frac{\partial W_z}{\partial z} + \frac{\partial W_y}{\partial y} = 0 \qquad (1)$$

$$\frac{\partial W_z}{\partial y} - \frac{\partial W_y}{\partial z} = 0 \qquad (2)$$

Consider the gas flow along a stream line in the mid part of the channel. The coordinates of the stream line and their differentials are related by,

$$S(z,y) = 0 \qquad (3)$$

$$\frac{\partial S}{\partial z} \cdot dz + \frac{\partial S}{\partial y} dy = 0 \qquad (4)$$

Following the motion of this stream line it is convenient to consider any quantity q on the stream line as a function of z only - i.e.

$$q = q\,[\,z,\ y(z)\,] \qquad (5)$$

$$\frac{dq}{dz} = \frac{\partial q}{\partial z} + \frac{\partial q}{\partial y} \cdot \frac{dy}{dz} \qquad (6)$$

and $$\frac{dy}{dz} = -\frac{\partial S/\partial z}{\partial S/\partial y} = \frac{W_y}{W_z} = \tan\beta \qquad (7)$$

hence, $$\frac{dq}{dz} = \frac{\partial q}{\partial z} + \frac{\partial q}{\partial y} \cdot \tan\beta \qquad (8)$$

from (1), (2) and (8)

$$\frac{dW_z}{dz} + \frac{\partial W_y}{\partial y} - \frac{\partial W_z}{\partial y}\tan\beta = 0 \qquad (9)$$

and $$\frac{dW_y}{dz} - \frac{\partial W_z}{\partial y} - \frac{\partial W_y}{\partial y}\tan\beta = 0 \qquad (10)$$

from equations (7), (9) and (10) the first partial derivatives can be written as,

$$\frac{\partial W_z}{\partial y} = \left(\frac{dW_y}{dz} + \frac{dW_z}{dz}\tan\beta\right)\mathrm{Cos}^2\beta \qquad (11)$$

$$\frac{\partial W_y}{\partial y} = \left(\frac{dW_y}{dz}\tan\beta - \frac{dW_z}{dz}\right)\mathrm{Cos}^2\beta \qquad (12)$$

to obtain the second derivatives; differentiating (1) with respect to y,

$$\frac{\partial^2(W_z)}{\partial z\,\partial y} + \frac{\partial^2(W_y)}{\partial y^2} = 0 \qquad (13)$$

from (8) and (13)

$$\frac{\partial^2 W_y}{\partial y^2} - \frac{\partial^2 W_z}{\partial y^2} \tan \beta + \frac{d}{dz} \left(\frac{\partial W_z}{\partial y}\right) = 0 \qquad (14)$$

differentiating (2) with respect to 'y' and using (8);

$$\frac{\partial^2 W_z}{\partial y^2} = \frac{d}{dz} \frac{\partial W_y}{\partial y} - \frac{\partial^2 W_y}{\partial y^2} \tan \beta \qquad (15)$$

from (9), (14) and (15)

$$\frac{\partial^2 W_y}{\partial y^2} = \left[\tan \beta . \frac{d}{dz} \left(\frac{\partial W_y}{\partial y}\right) - \frac{d}{dz} \left(\frac{\partial W_z}{\partial y}\right) \right] \cos^2 \beta \qquad (16)$$

from (16) and (14)

$$\frac{\partial^2 W_z}{\partial y^2} = \left[\frac{d}{dz} \left(\frac{\partial W_y}{\partial y}\right) - \frac{\partial^2 W_y}{\partial y^2} \tan \beta \right]$$

$$= \left[\frac{d}{dz} \left(\frac{\partial W_y}{\partial y}\right) + \frac{d}{dz} \left(\frac{\partial W_z}{\partial y}\right) \tan \beta \right] \cos^2 \beta \qquad (17)$$

APPENDIX 'B' (Ref. |17|)

The total pressure for incompressible flow at some point in the boundary-layer is

$$P_{oi} = p_i + 1/2\ \rho\ W_i^2 \qquad (1)$$

Where, the subscript 'i' denotes the values at the point under consideration within the boundary layer. The total pressure in the freestream is,

$$P_{ot.e.} = p + 1/2\ \rho\ W_{t.e.}^2 \qquad (2)$$

For an uniform discharge static pressure, the loss in total pressure at some point in the boundary-layer at the trailing edge is given by,

$$\Delta P_{oi} = 1/2\ \rho (W_{t.e.}^2 - W_i^2) \qquad (3)$$

Integrating this loss across one blade passage at the trailing edge and weighing for flow,

$$\int_0^t (\Delta P_{oi})\ W_{zi}\ dt = \int_0^t \frac{\rho}{2} (W_{t.e.}^2 - W_i^2)\ W_{zi}\ dt \qquad (4)$$

and $$\Delta P_{ot.e.} = \frac{\int_0^t (\Delta P_{c1})\, W_{zi}\, dt}{W_z\, t}$$

$$= \frac{\int_0^t \frac{\rho}{2} (W^2_{t.e.} - W_i^2)\, W_{zi}\, dt}{W_z\, t} \qquad (5)$$

Where $\Delta P_{ot.e.}$ W_z are the average values of pressure loss and axial velocity respectively.

Now define the loss coefficient, ζ_v, as,

$$\zeta_v = \frac{\Delta P_{ot.e.}}{1/2 \rho W_z^2} = \frac{1}{t \cos^2 \beta_2} \int_0^t \left(1 - \frac{W_i^2}{W^2_{t.e.}}\right) \frac{W_{zi}}{W_{t.e.}}\, dt \qquad (6)$$

define the energy thickness as

$$1/2 \rho W^3_{t.e.} \phi_1 = \frac{1}{2} \rho \int_0^\delta (W^3_{t.e.} - W_i^3)\, dy \qquad (7)$$

This form follows directly from the consideration of the deficiency of kinetic energy of a stream of profile W_1 referred to one of constant velocity $W_{t.e.}$. In particular, if $W_{t.e.}$ is the mean outflow velocity and the integration is carried over the pitch of the cascade, the continuity equation

$$\int_0^t W_{t.e.}\, dy = \int_0^t W_i\, dy \qquad (8)$$

allows it to be written as

$$\phi_1 = \int_0^t \frac{W_1}{W_{t.e.}} \left[1 - \left(\frac{W_i}{W_{t.e.}} \right)^2 \right] dy \qquad (9)$$

where, ϕ_1 represents the energy lost per unit breadth and unit time.

From (6) and (9)

$$\zeta_v = \frac{W_{t.e.}}{W_z} \frac{\phi_1}{t} \cdot \frac{1}{\cos^2 \beta_2} = \frac{\phi_1}{t \cos^3 \beta_2} \qquad (10)$$

If the energy lost is taken to be equal to the work done by the shear forces, then,

$$\frac{1}{2} W_{t.e.}^3 \phi_1 = W_{t.e.} \int_0^L \tau_o \, dx \qquad (11)$$

using Von Karman's integral equation,

$$\frac{\tau_o}{\rho W_{t.e.}^2} = \frac{d\theta}{dx} + \frac{(H+2)}{W_{t.e.}} \theta \frac{dW_{t.e.}}{dx} \qquad (12)$$

H = form factor = displacement thickness/momentum thickness

τ_o = shear stress at the wall

Eqn. (12) can be written as,

$$\frac{1}{2}\rho W_{t.e.}^3 \phi_1 = W_{t.e.} \int_0^L \left[\frac{d}{dx} (\rho W_{t.e.}^2 \theta) + \rho W_{t.e.}^2 \frac{H+2}{W_{t.e.}} \cdot \frac{dW_{t.e.}}{dx} \right] dx \qquad (13)$$

assuming the velocity gradient to be negligible at the t.e., the above equation can be written as,

$$\frac{1}{2} \rho W_{t.e.}^3 \phi_1 = \rho W_{t.e.}^3 \theta_L \quad [\because \theta_o = 0.] \qquad (14)$$

θ_o = momentum thickness at the leading edge.

θ_L = momentum thickness at the trailing edge.

From (14)

$$\phi_1 \mid \theta = 2 \qquad (15)$$

From (10) and (15),

$$\zeta_v = \frac{2\theta}{t \cos^3 \beta_2} \qquad (16)$$

where β_2 is the outlet angle for the real flow.

APPENDIX 'C'

THE FOLLOWING AIRFOILS ARE TESTED IN CASCADES AND THE DETAILS ARE AS UNDER :—

	DESIGN INLET ANGLE	CAMBER ANGLE	CHORD LENGTH
BLADE NO 1	51°	96 5°	4 IN
BLADE NO 2	60 5°	90.0°	4 IN
BLADE NO 3	61 5°	87 5°	4 IN
BLADE NO 4	31 5°	51 5°	4 IN

BLADES 1 TO 3 ARE TESTED FOR VARIOUS COMBINATIONS OF $\lambda = 0°$, 5° & 15° AND PITCH-CHORD RATIOS OF .5/4 & 5 0/4 0 . IN THE CASE OF BLADE NO 4 λ IS NEGATIVE

BLADE NO. 1

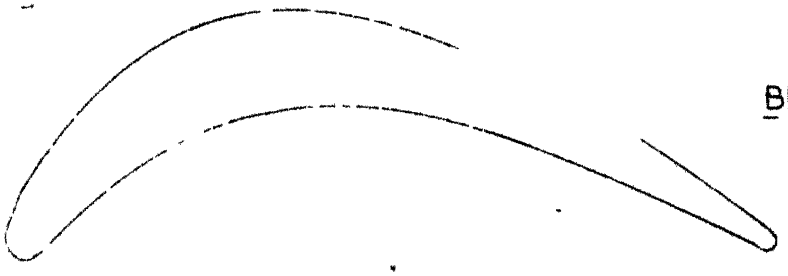

BLADE NO. 2

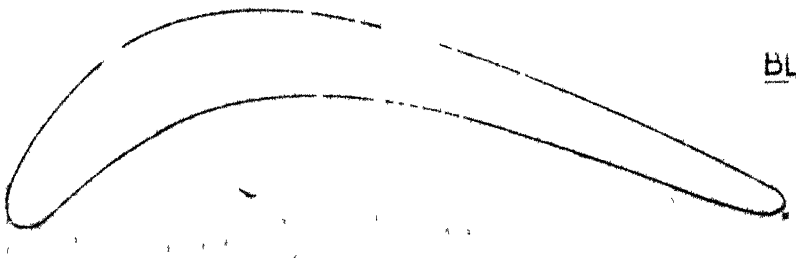

BLADE NO 3

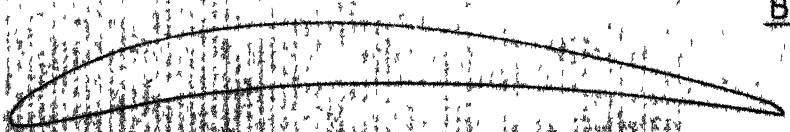

BLADE NO. 4

TABLES 1 AND 2

BLADE No. 1

(See Appendix 'C')

Stagger = + 15° α = 0.659 t/L = 3.0/4.0

Reference Velocity = 41.59 m./sec.

S.No.	% chord	Suction Surface		Pressure surface	
		$C_{pTH.}$	$C_{pEXP.}$	$C_{pTH.}$	$C_{pEXP.}$
1	0.1	-1.005	-1.003	+0.717	+0.662
2	0.2	-1.505	-1.208	+0.749	+0.719
3	0.3	-1.075	-1.144	+0.781	+0.798
4	0.4	-0.705	-0.743	+0.758	+0.846
5	0.5	-0.555	-0.498	+0.748	+0.797
6	0.6	-0.465	-0.355	+0.698	+0.739
7	0.7	-0.345	-0.305	+0.596	+0.654
8	0.8	-0.255	-0.193	+0.526	+0.556
9	0.9	-0.083	-0.077	+0.412	+0.367
10	1.0	+0.209	-0.023	+0.235	+0.158

BLADE NO.3 (See Appendix 'C')

Stagger = + 15° α = 0.681 t/L = 3.0/4.0

Reference Velocity = 41.39 m./sec.

1	0.1	-1.105	-0.878	+0.516	+0.641
2	0.2	-1.849	-1.401	+0.467	+0.691
3	0.3	-0.905	-1.310	+0.688	+0.847
4	0.4	-0.692	-1.186	+0.664	+0.827
5	0.5	-0.535	-1.100	+0.621	+0.808
6	0.6	-0.540	-0.772	+0.558	+0.748
7	0.7	-0.570	-0.533	+0.510	+0.639
8	0.8	-0.559	-0.425	+0.459	+0.526
9	0.9	-0.575	-0.242	+0.342	+0.341
10	1.0	-0.438	-0.087	+0.419	+0.088

TABLES 3 AND 4

BLADE No.2 (See Appendix 'C')

Stagger angle = 15° t/L = 3.0/4.0

Reference velocity = 41.012 m./sec. α = 0.634

S.No.	% chord	Suction surface		Pressure surface	
		$C_{pTH.}$	$C_{pEXP.}$	$C_{pTH.}$	$C_{pEXP.}$
1	0.1	-1.56	-1.37	+0.65	+0.59
2	0.2	-1.94	-1.75	+0.62	+0.65
3	0.3	-1.27	-1.17	+0.77	+0.77
4	0.4	-1.15	-1.10	+0.76	|0.72
5	0.5	-0.50	-0.40	+0.69	+0.61
6	0.6	-0.45	-0.37	+0.60	+0.55
7	0.7	-0.37	-0.27	+0.48	+0.44
8	0.8	-0.31	-0.21	+0.41	+0.37
9	0.9	-0.08	-0.12	+0.29	+0.19
10	1.0	+0.12	+0.08	+0.32	+0.12

Blade No.4 Stagger angle = -15° t/L = 3.0/4.0

Reference velocity = 39.4 m./sec. α = 0.707

1	0.1	-0.662	-1.402	+0.000	+0.148
2	0.2	-1.162	-1.112	+0.069	+0.168
3	0.3	-1.202	-0.730	+0.164	+0.188
4	0.4	-0.890	-0.520	+0.199	+0.190
5	0.5	-0.745	-0.372	+0.200	+0.212
6	0.6	-0.542	-0.299	+0.268	+0.220
7	0.7	-0.670	-0.280	+0.380	+0.242
8	0.8	-0.340	-0.275	+0.342	+0.380
9	0.9	+0.055	-0.040	+0.294	+0.305
10	1.0	+0.212	+0.175	+0.249	+0.264

TABLES 5 AND 6

BLADE NO.1

(See Appendix 'C')

Stagger = $+0^{\circ}$ $\alpha = 0.694$ $t/L = 2.5/4.0$

Reference Velocity = 40.75 m./sec.

S.No.	% Chord	Suction Surface		Pressure Surface	
		C_{pTH}	C_{pEXP}	C_{pTH}	C_{pEXP}
1	0.1	-1.700	-1.449	-0.015	+0.032
2	0.2	-2.482	-1.512	+0.375	+0.119
3	0.2	-2.299	-2.015	+0.606	+0.382
4	0.4	-1.465	-2.002	+0.392	+0.543
5	0.5	-1.312	-1.812	+0.439	+0.512
6	0.6	-1.155	-1.312	+0.512	|0.485
7	0.7	-1.025	-0.835	+0.349	+0.252
8	0.8	-0.889	-0.410	+0.331	+0.191
9	0.9	-0.635	-0.202	+0.242	+0.016
10	1.0	-0.015	-0.210	-0.001	-0.092

BLADE NO.1 (See Appendix 'C')

Stagger = + 5° $\alpha = 0.675$ $t/L = 2.5/4.0$

Reference Velocity = 39.66 m./sec.

1	0.1	-0.758	-1.664	+0.371	+0.492
2	0.2	-0.694	-1.588	+0.275	+0.587
3	0.3	-0.539	-1.151	+0.287	+0.612
4	0.4	-0.482	-1.562	+0.348	+0.704
5	0.5	-0.365	-1.382	+0.356	+0.726
6	0.6	-0.292	-1.302	+0.407	+0.674
7	0.7	-0.262	-1.151	+0.321	+0.587
8	0.8	-0.204	-0.621	+0.233	+0.510
9	0.9	-0.142	-0.362	+0.039	+0.334
10	1.0	-0.222	-0.350	-0.166	-0.009

TABLES 7 AND 8

BLADE No. 2

(See Appendix 'C')

Stagger = 0° α = 0.735 t/L = 2.5/4.0

Reference Velocity = 41.35 m./sec.

S.No.	% chord	Suction Surface		Pressure Surface	
		C_{pTH}	C_{pEXP}	C_{pTH}	C_{pEXP}
1	0.1	-2.645	-2.655	-0.282	+0.132
2	0.2	-2.822	-2.945	-0.018	+0.718
3	0.3	-1.645	-1.749	+0.458	+0.735
4	0.4	-1.605	-1.652	+0.362	+0.697
5	0.5	-0.892	-0.982	+0.245	+0.354
6	0.6	-0.782	-0.682	+0.149	+0.308
7	0.7	-0.822	-0.575	+0.155	+0.168
8	0.8	-0.735	-0.415	+0.078	+0.109
9	0.9	-0.652	-0.382	+0.030	-0.021
10	1.0	-0.365	-0.368	-0.160	-0.161

Stagger = $+5^{\circ}$ α = 0.735 BLADE No. 2 (See Appendix 'C') t/L = 2.5/4.0

Reference Velocity = 40.77 m./sec.

1	0.1	-0.815	-1.898	+0.207	+0.141
2	0.2	-1.649	-1.720	+0.439	+0.251
3	0.3	-1.382	-1.602	+0.471	+0.451
4	0.4	-0.972	-1.401	+0.457	+0.552
5	0.5	-0.905	-0.876	+0.372	+0.529
6	0.6	-0.815	-0.762	+0.271	+0.451
7	0.7	-0.412	-0.771	+0.246	+0.309
8	0.8	-0.419	-0.519	+0.187	+0.289
9	0.9	-0.065	-0.520	+0.164	+0.232
10	1.0	-0.021	-0.535	+0.077	+0.109

TABLES 9 AND 10

BLADE No.3

(See Appendix 'C')

Stagger = 0° $\alpha = 0.752$ t/L = 2.5/4.0

Reference Velocity = 41.40 m./sec.

S.No.	%	Suction Surface C_{pTH}	Suction Surface C_{pEXP}	Pressure Surface C_{pTH}	Pressure Surface C_{pEXP}
1	0.1	-2.725	-2.355	-0.175	+0.272
2	0.2	-3.062	-2.331	+0.462	+0.636
3	0.3	-2.065	-2.585	+0.442	+0.646
4	0.4	-1.399	-2.262	+0.505	+0.665
5	0.5	-1.089	-1.146	+0.526	+0.546
6	0.6	-0.733	-1.001	+0.437	+0.515
7	0.7	-0.882	-0.619	+0.258	+0.389
8	0.8	-0.842	-0.285	+0.212	+0.250
9	0.9	-0.342	-0.316	+0.112	+0.092
10	1.0	-0.099	-0.272	+0.082	-0.139

BLADE NO. 3 (See Appendix 'C')

Stagger = 5° $\alpha = 0.736$ t/L = 2.5/4.0

Reference Velocity = 41.40 m./sec.

1	0.1	-1.404	-2.406	+0.021	+0.722
2	0.2	-1.299	-2.455	+0.162	+0.731
3	0.3	-0.475	-2.498	+0.502	+0.788
4	0.4	-0.565	-1.199	+0.412	+0.711
5	0.5	-0.439	-1.024	+0.448	+0.564
6	0.6	-0.369	-0.052	+0.449	+0.427
7	0.7	-0.374	-0.041	+0.519	+0.385
8	0.8	-0.299	-0.152	+0.346	+0.296
9	0.9	-0.260	-0.161	+0.308	+0.164
10	1.0	-0.198	-0.142	+0.453	+0.089

TABLES 11 AND 12

BLADE NO.1

(See Appendix 'C')

Stagger = + 0° α = 0.715 t/L = 3.0/4.0

Reference Velocity = 40.34 m./sec.

S.No.	% chord	Suction Surface		Pressure Surface	
		C_{pTH}	C_{pEXP}	C_{pTH}	C_{pEXP}
1	0.1	-1.901	-1.685	+0.321	+0.061
2	0.2	-2.845	-1.772	+0.444	+0.142
3	0.3	-2.745	-2.298	+0.715	+0.421
4	0.4	-1.710	-2.205	+0.474	+0.584
5	0.5	-1.260	-2.075	+0.568	+0.552
6	0.6	-1.455	-1.572	+0.652	+0.521
7	0.7	-1.052	-1.105	+0.497	+0.472
8	0.8	-0.942	-0.741	+0.498	+0.417
9	0.9	-0.619	-0.781	+0.429	+0.252
10	1.0	+0.051	-0.740	+0.189	+0.101

BLADE NO. 1 (See Appendix 'C')

Stagger = + 5° α = 0.705 t/L = 3.0/4.0

Reference Velocity = 39.29 m./sec.

1	0.1	-0.785	-1.914	+0.358	+0.539
2	0.2	-1.452	-1.845	+0.209	+0.635
3	0.3	-2.098	-1.752	+0.292	+0.655
4	0.4	-1.103	-1.820	+0.391	+0.753
5	0.5	-0.579	-1.635	+0.429	+0.774
6	0.6	-0.498	-1.548	+0.394	+0.720
7	0.7	-0.342	-1.261	+0.142	+0.635
8	0.8	-0.286	-0.942	+0.069	+0.445
9	0.9	-0.219	-0.902	-0.027	+0.332
10	1.0	-0.158	-0.825	-0.046	+0.092

TABLES 13 AND 14

BLADE NO.2

(See Appendix 'C')

Stagger = 0^{o} α = 0.751 t/L = 3.0/4.0

Reference Velocity = 40.73 m./sec.

S.No.	% chord	Suction Surface		Pressure Surface	
		C_{pTH}	C_{pEXP}	C_{pTH}	C_{pEXP}
1	0.1	-2.301	-2.649	-0.102	+0.482
2	0.2	-2.562	-2.589	+0.555	+0.687
3	0.3	-3.146	-2.862	+0.531	+0.696
4	0.4	-1.602	-2.549	+0.482	+0.765
5	0.5	-1.355	-1.800	+0.482	+0.596
6	0.6	-0.875	-1.225	+0.440	+0.566
7	0.7	-0.611	-0.768	+0.442	+0.482
8	0.8	-0.743	-0.385	+0.418	+0.355
9	0.9	-0.524	-0.342	+0.098	+0.242
10	1.0	-0.221	-0.378	+0.071	+0.096
Stagger = $+5^{o}$		α = 0.750	t/L = 3.0/4.0		
		Reference Velocity = 40.45 m./sec.			
1	0.1	-0.074	-2.150	+0.331	+0.168
2	0.2	-1.405	-1.962	+0.198	+0.281
3	0.3	-2.152	-2.742	+0.274	+0.482
4	0.4	-1.085	-2.062	+0.358	+0.585
5	0.5	-0.485	-1.851	+0.348	+0.565
6	0.6	-0.468	-1.109	+0.330	+0.482
7	0.7	-0.305	-0.709	+0.186	+0.446
8	0.8	-0.329	-0.545	+0.121	+0.342
9	0.9	-0.239	-0.550	+0.074	+0.195
10	1.0	-0.059	-0.525	+0.016	+0.059

TABLES 15 AND 16

BLADE No.3

(See Appendix 'C')

Stagger = $+0^{o}$ α = 0.705 t/L = 3.0/4.0

Reference Velocity = 41.36 m./sec.

S.No.	%	Suction Surface		Pressure Surface	
		C_{pTH}	C_{pEXP}	C_{pTH}	C_{pEXP}
1	0.1	-3.361	-1.701	+0.071	-0.166
2	0.2	-3.725	-2.725	+0.545	-0.046
3	0.3	-2.585	-2.730	+0.498	+0.051
4	0.4	-1.698	-1.415	+0.458	+0.159
5	0.5	-1.291	-1.199	+0.678	+0.297
6	0.6	-0.821	-1.062	+0.554	+0.308
7	0.7	-1.021	-1.001	+0.372	+0.258
8	0.8	-0.965	-0.541	+0.432	+0.179
9	0.9	-0.385	-0.482	+0.241	+0.148
10	1.0	-0.089	-0.479	+0.436	+0.072

Stagger = $+5^{o}$ BLADE No.3 (See Appendix 'C')

α = 0.746 t/L = 3.0/4.0

Reference Velocity = 40.98 m./sec.

1	0.1	-2.155	-2.655	+0.034	+0.562
2	0.2	-1.948	-2.743	+0.114	+0.764
3	0.3	-0.719	-2.845	+0.212	+0.774
4	0.4	-0.682	-1.440	+0.349	+0.838
5	0.5	-0.828	-1.245	+0.492	+0.755
6	0.6	-0.512	-0.731	+0.484	+0.605
7	0.7	-0.601	-0.563	+0.438	+0.465
8	0.8	-0.705	-0.515	+0.359	+0.341
9	0.9	-1.198	-0.389	+0.308	+0.192
10	1.0	-0.384	-0.398	+0.132	+0.081

TABLES 17 AND 18

BLADE NO.4

(See Appendix 'C')

Stagger angle = 0° t/L = 2.5/4.0

Reference velocity = 39.614 m./sec. α = 0.516

S.No.	% chord	Suction surface		Pressure surface	
		$C_{pTH.}$	$C_{pEXP.}$	$C_{pTH.}$	$C_{pEXP.}$
1	0.1	-0.664	-0.614	-0.132	-0.231
2	0.2	-1.158	-0.962	+ 0.086	+ 0.202
3	0.3	-1.062	-0.804	+ 0.133	+ 0.204
4	0.4	-0.602	-0.428	+ 0.172	+ 0.252
5	0.5	-0.604	-0.371	+ 0.144	+ 0.241
6	0.6	-0.473	- 0.304	+ 0.146	+ 0.235
7	0.7	-0.421	-0.182	+ 0.104	+ 0.103
8	0.8	-0.375	-0.124	+ 0.002	+ 0.001
9	0.9	-0.024	+0.136	- 0.103	- 0.076
10	1.0	+0.086	+0.104	- 0.018	- 0.042
	Stagger angle = -5° t/L = 2.5/4.0 Reference velocity = 40.032 m./sec. α = 0.517				
1	0.1	-0.721	-0.582	- 0.452	- 0.455
2	0.2	-1.214	-0.918	+ 0.028	- 0.102
3	0.3	-1.308	-1.049	+ 0.069	- 0.024
4	0.4	-0.589	-0.424	+ 0.184	+ 0.218
5	0.5	-0.536	-0.358	+ 0.309	+ 0.269
6	0.6	-0.468	-0.379	+ 0.424	+ 0.379
7	0.7	-0.412	-0.392	+ 0.308	+ 0.328
8	0.8	-0.243	-0.184	+ 0.079	+ 0.042
9	0.9	-0.209	-0.152	+ 0.012	+ 0.014
10	1.0	-0.089	-0.031	- 0.015	+ 0.012

TABLES 19 AND 20

BLADE NO. 4

Stagger = 0° t/L = 3.0/4.0

Reference velocity = 39.604 m./sec. α = 0.517

S.No.	% chord	Suction surface		Pressure surface	
		$C_{pTH.}$	$C_{pEXP.}$	$C_{pTH.}$	$C_{pEXP.}$
1	0.1	-0.782	-1.214	-0.012	+0.085
2	0.2	-1.442	-1.345	+0.122	+0.205
3	0.3	-1.300	-1.155	+0.151	+0.139
4	0.4	-0.730	-0.652	+0.228	+0.205
5	0.5	-0.680	-0.530	+0.235	+0.242
6	0.6	-0.460	-0.350	+0.208	+0.169
7	0.7	-0.326	-0.284	+0.110	+0.090
8	0.8	-0.103	-0.102	+0.062	+0.025
9	0.9	+0.058	+0.062	-0.102	-0.062
10	1.0	+0.085	+0.085	-0.044	+0.016
	Stagger = -5°	t/L = 3.0/4.0			
	Reference velocity = 40.021 m./sec.	α = 0.620			
1	0.1	-0.872	-1.102	-0.420	-0.382
2	0.2	-1.452	-1.355	+0.010	+0.120
3	0.3	-1.624	-1.290	+0.340	+0.345
4	0.4	-0.745	-0.620	+0.429	+0.452
5	0.5	-0.642	-0.579	+0.455	+0.494
6	0.6	-0.620	-0.395	+0.505	+0.584
7	0.7	-0.569	-0.380	+0.309	+0.392
8	0.8	-0.382	-0.164	+0.110	+0.232
9	0.9	-0.292	-0.202	-0.010	+0.088
10	1.0	-0.379	+0.042	-0.058	+0.101

TABLE 21

S.No.	Blade No.		t/L	θ_{TH} Suction Surface	Pressure Surface	Profile Loss T_{Ho} coeft.	Total Loss Coeft.
1	2	0^o	2.5/1.0	43.26	7.14	0.1083	0.2142
2	2	$+5^o$	2.5/4.0	33.13	7.44	0.1029	0.2092
3	2	0^o	3.0/4.0	33.17	6.38	0.0968	0.2208
4	2	$+5^o$	3.0/4.0	35.60	9.31	0.1103	0.2125
5	3	0^o	2.5/4.0	34.59	9.57	0.1015	0.2225
6	3	$+5^o$	2.5/4.0	38.96	8.41	0.1000	0.2082
7	3	0^o	3.0/4.0	33.01	6.75	0.0924	0.2322
8	3	$+5^o$	3.0/4.0	40.71	5.51	0.0969	0.2192
9	1	0^o	3.0/4.0	27.80	4.65	0.1011	0.2148
10	1	$+5^o$	3.0/4.0	38.09	5.53	0.0971	0.2084
11	4	-15^o	3.0/1.0	41.52	8.73	0.0386	0.0780

TABLE 22

l. No.	Blade No.		t/L	$\theta_{TH.}$ Suction Surface	$\theta_{TH.}$ Pressure Surface	$\theta_{EXP.}$ Suction Surface	$\theta_{EXP.}$ Pressure Surface	Profile Loss Coeft. TH.	Profile Loss Coeft. EXP.	Total Loss Coeft.
2	4	-0°	2.5/4.0	22.2.	4.99	18.16	4.02	0.0240	0.0210	0.0341
3	4	-5°	2.5/4.0	21.93	5.11	21.65	4.20	0.0258	0.0228	0.0407
4	4	0°	3.0/4.0	24.24	7.07	24.52	4.26	0.0244	0.0228	0.0461
5	4	-5°	3.0/4.0	25.95	7.07	25.77	4.13	0.0265	0.0236	0.051
16	1	0°	2.5/4.0	36.27	7.26	46.34	13.29	0.0633	0.0867	0.202
17	1	$+5^{\circ}$	2.5/4.0	30.37	5.76	41.25	13.29	0.0646	0.0970	0.198
18	1	$+15^{\circ}$	3.0/4.0	29.65	4.47	26.15	9.62	0.0974	0.1021	0.1650
19	2	$+15^{\circ}$	3.0/4.0	37.02	7.01	37.34	11.87	0.0829	0.0927	0.1764
20	3	$+15^{\circ}$	3.0/4.0	46.16	7.23	41.25	13.29	0.0956	0.0976	0.1812

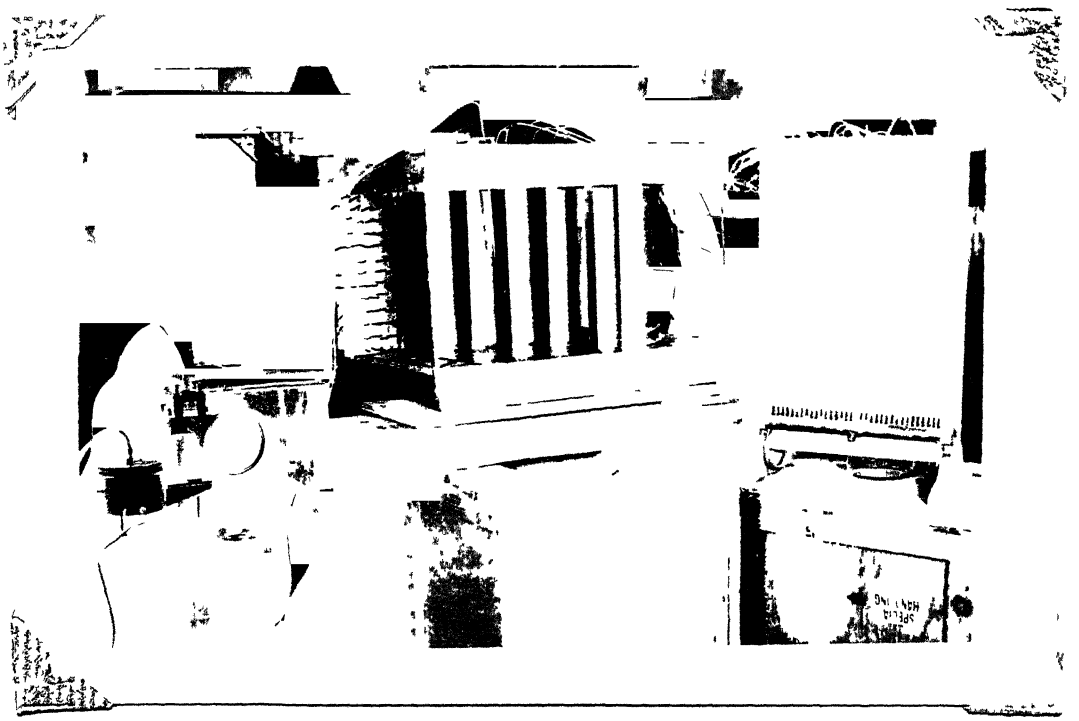

FIG I_EXPERIMENTAL SET UP

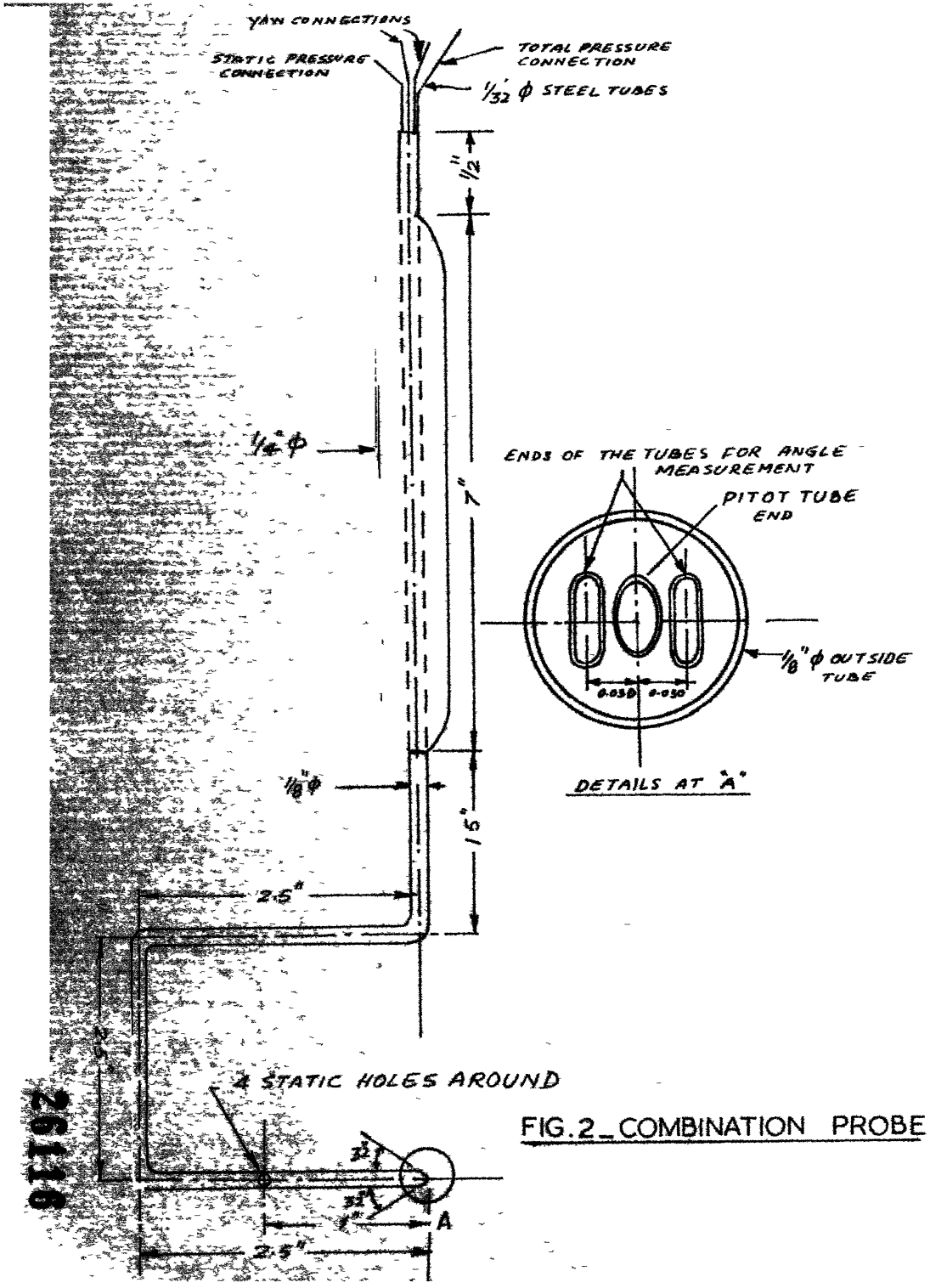

FIG. 2_COMBINATION PROBE

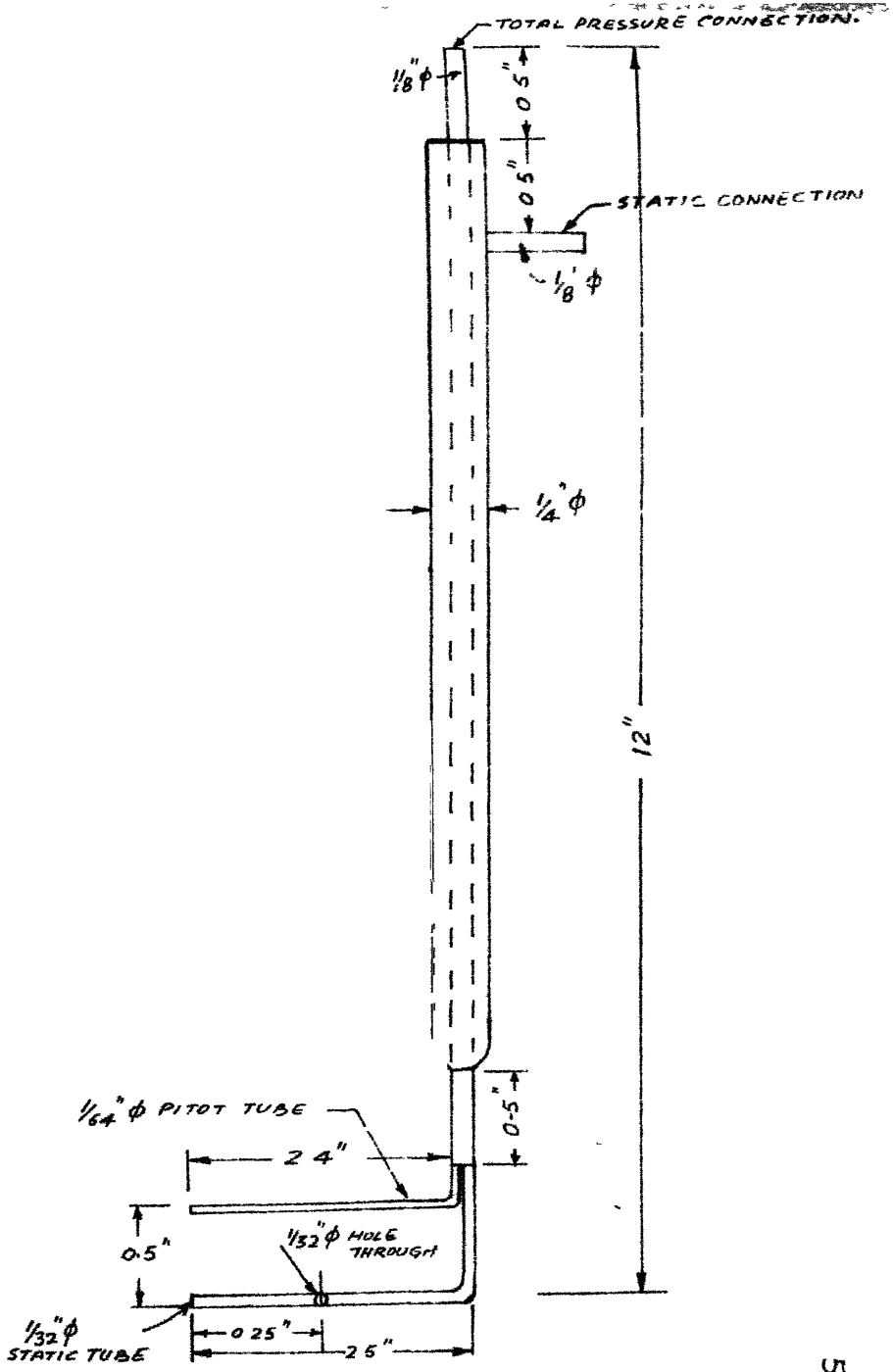

FIG 3_BOUNDARY LAYER PROBE

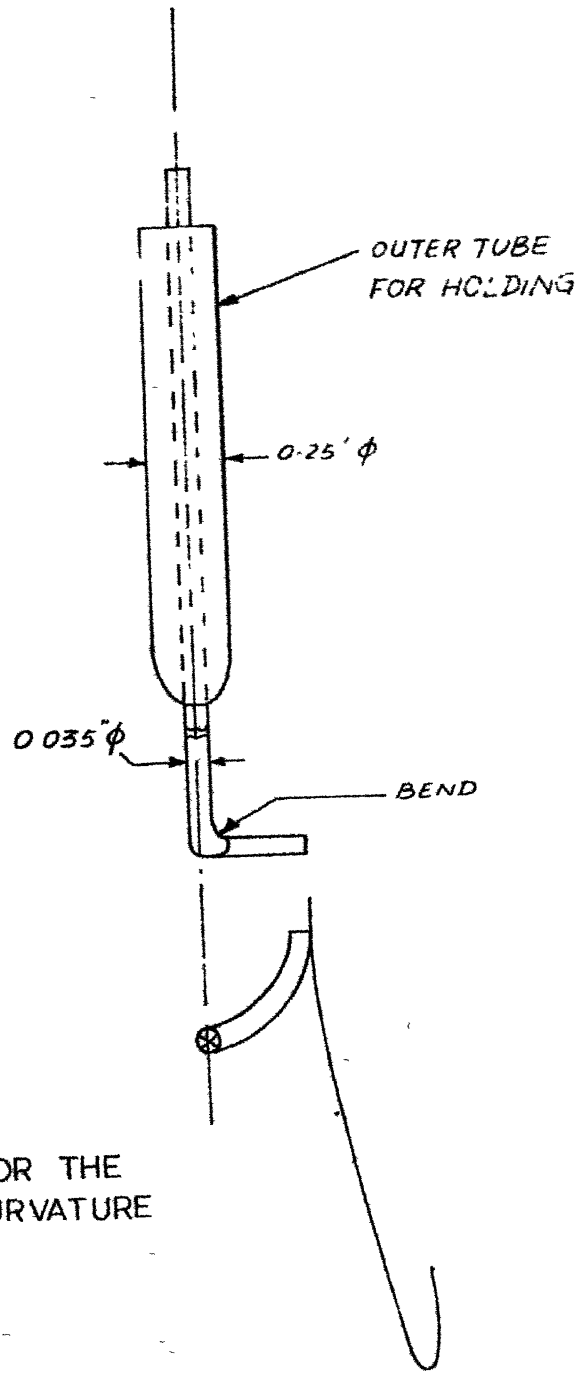

PROBE FOR THE
UPPER CURVATURE

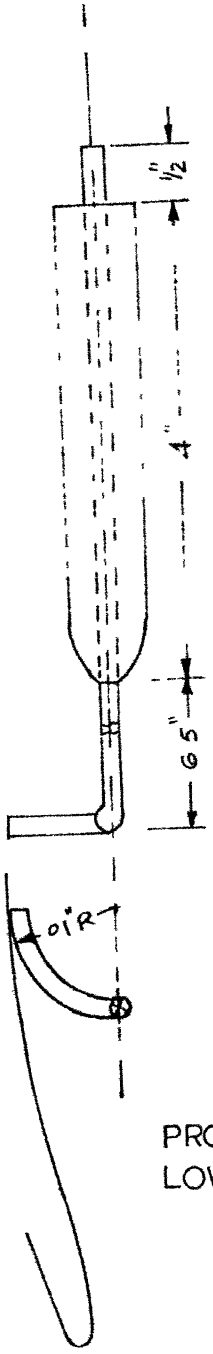

PROBE FOR THE
LOWER CURVATURE

FIG. 4

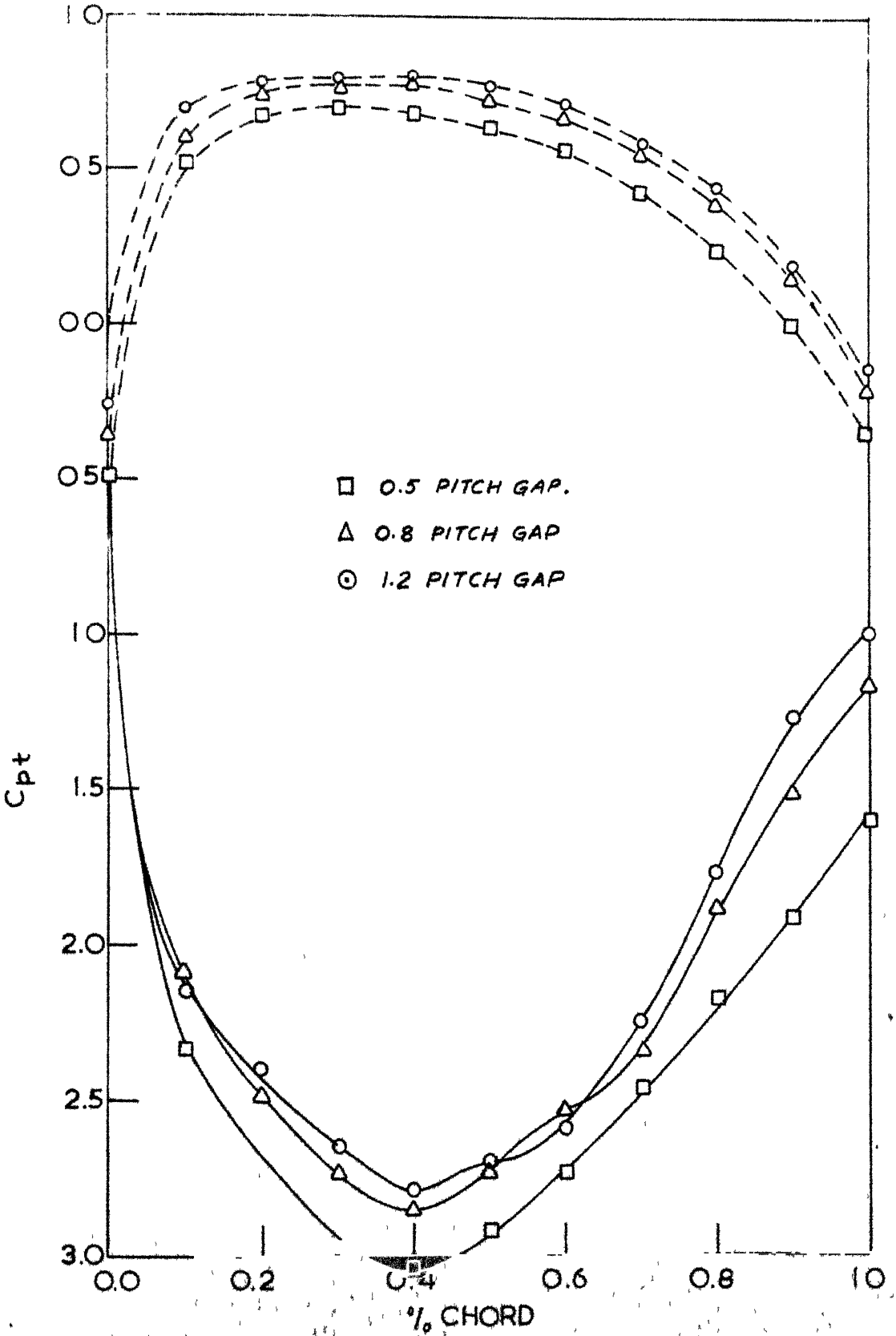

FIG.5 EFFECT OF END VANES

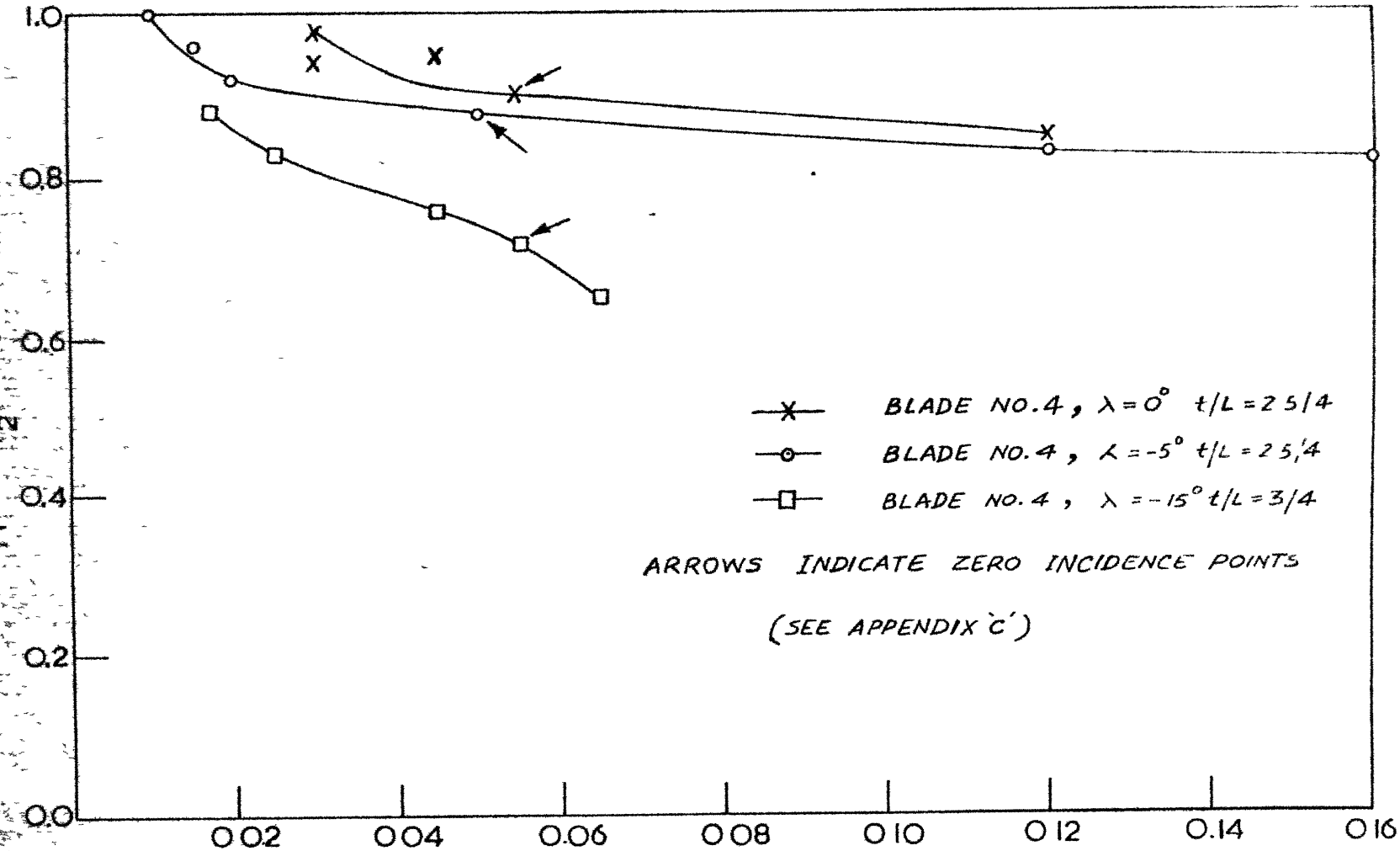

$\frac{W_{32} - W_{31}}{W_{31}}$ CONTRACTION COEFFICIENT

FIG 6_ CONTRACTION COEFFICIENTS

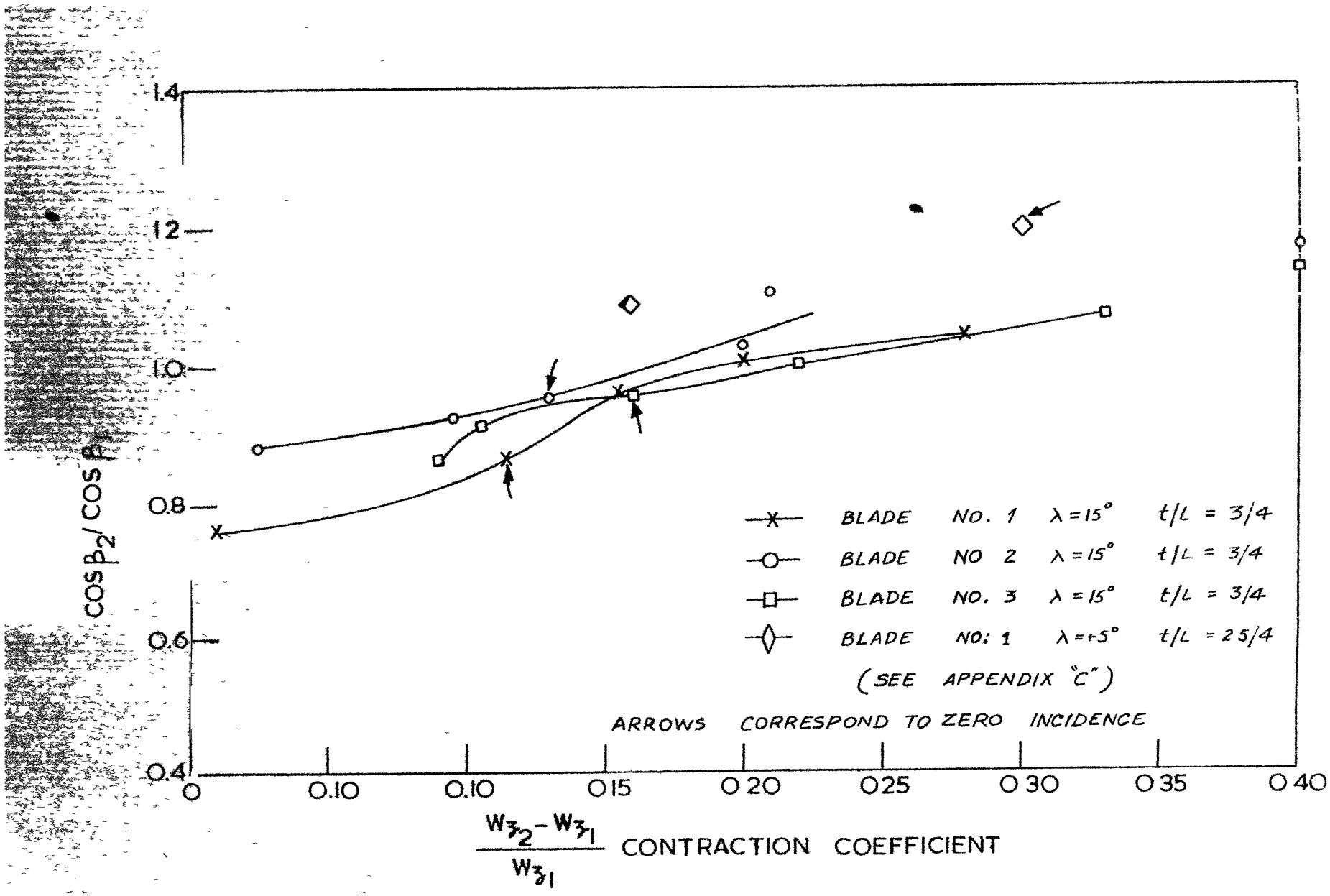

FIG 7_CONTRACTION COEFFICIENTS

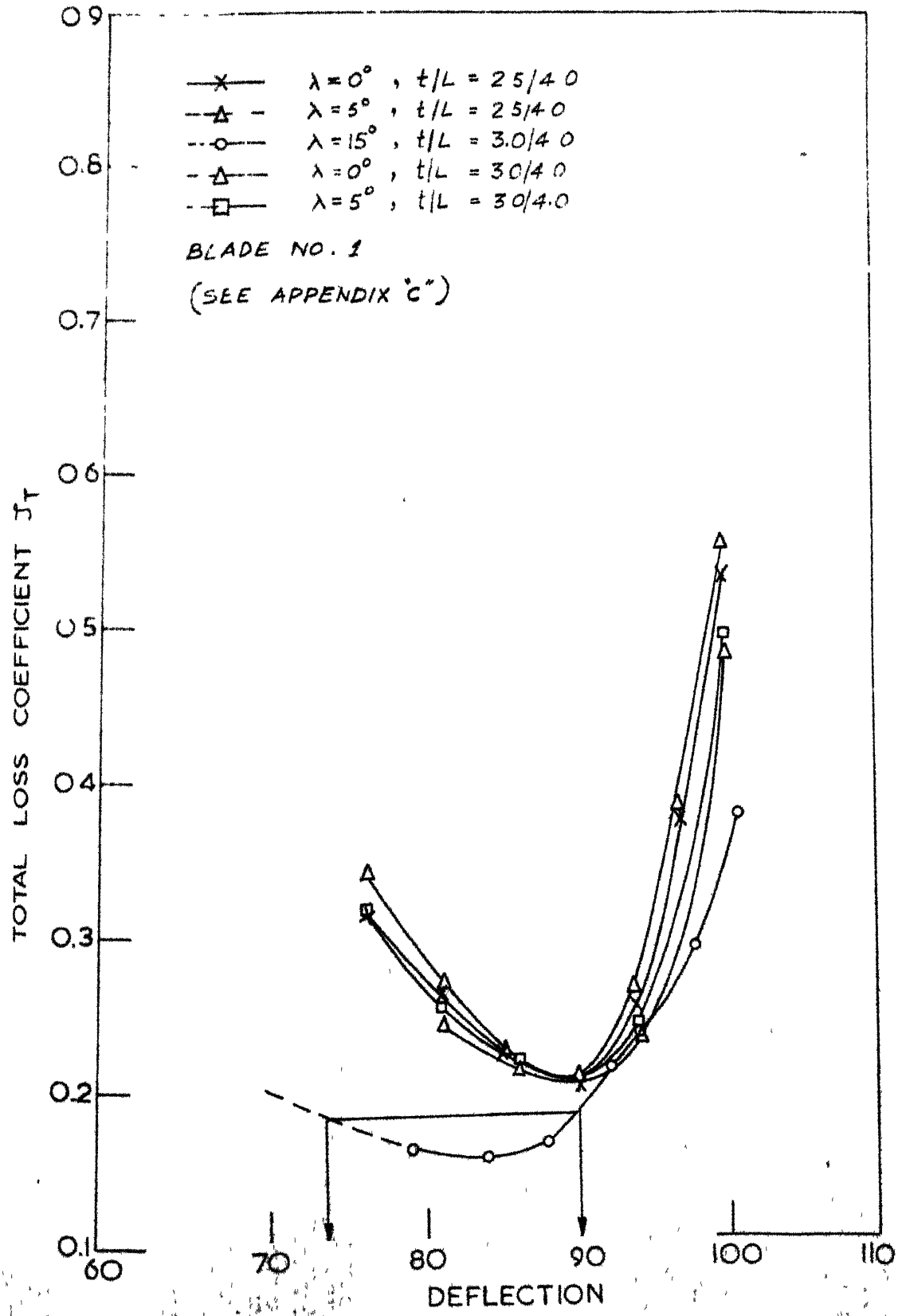

FIG. 8 – TOTAL LOSS COEFFICIENT Vs DEFLECTION

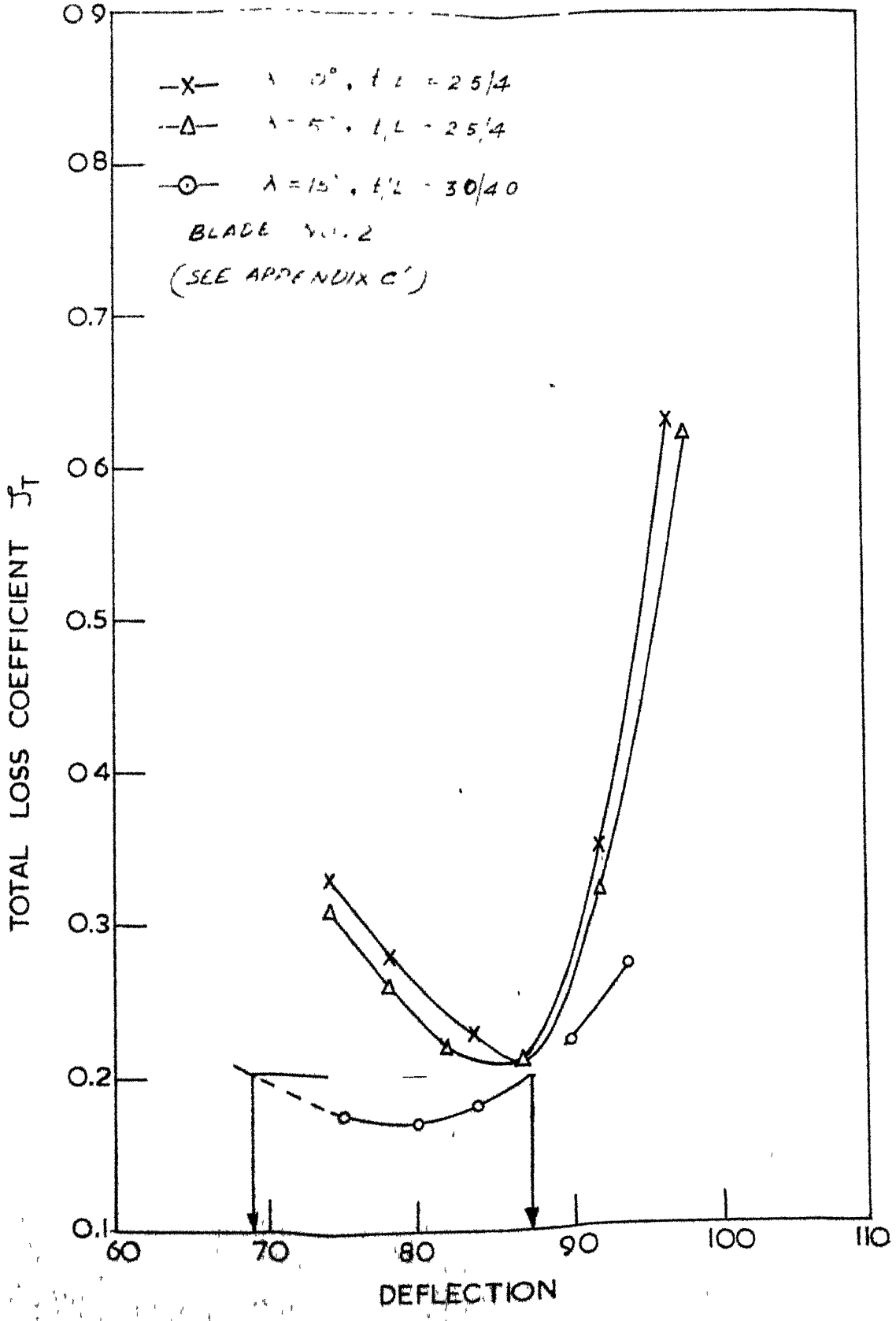

FIG.9 TOTAL LOSS COEFFICIENT VS. DEFLECTION

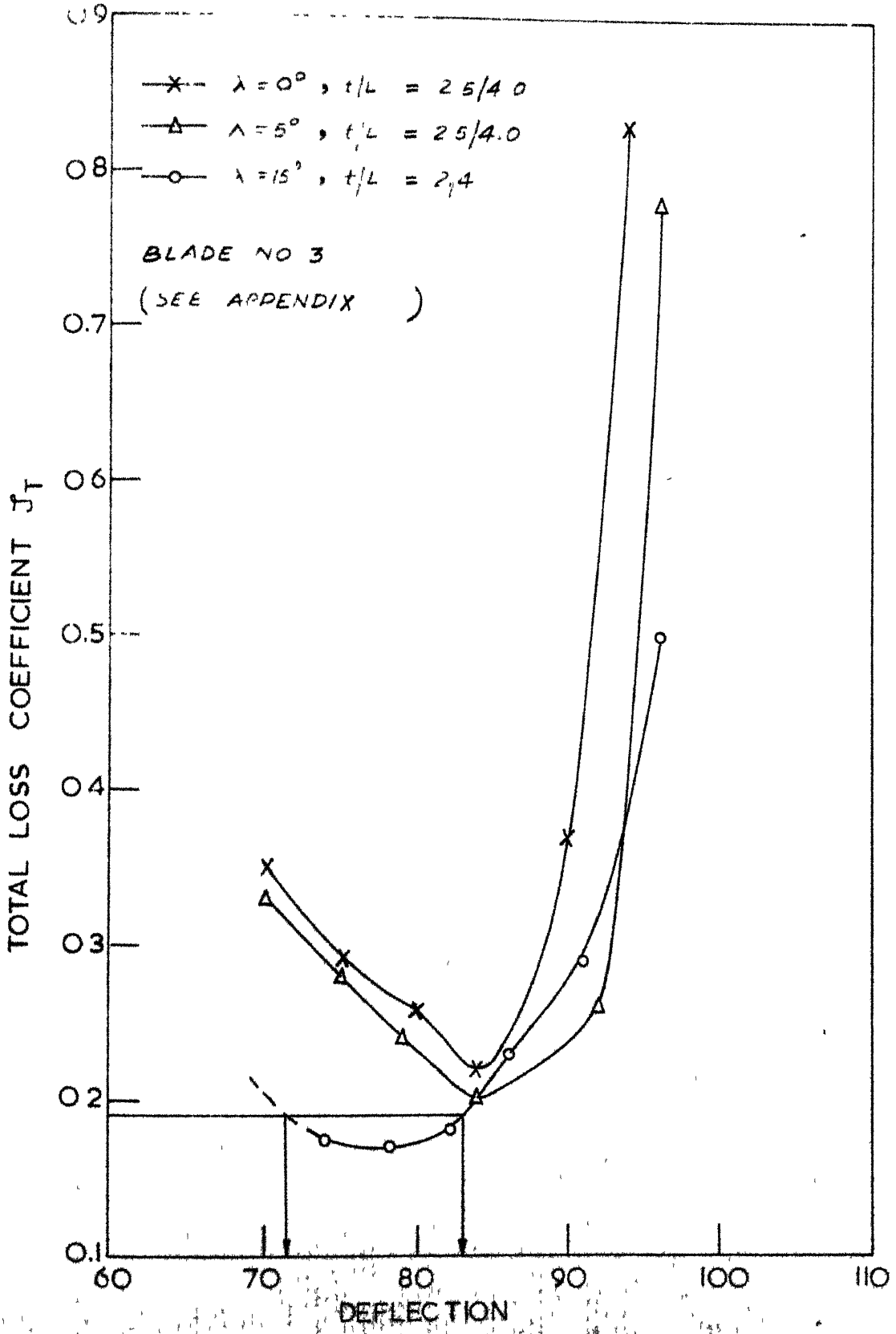

FIG.10- TOTAL LOSS COEFFICIENT VS DEFLECTION

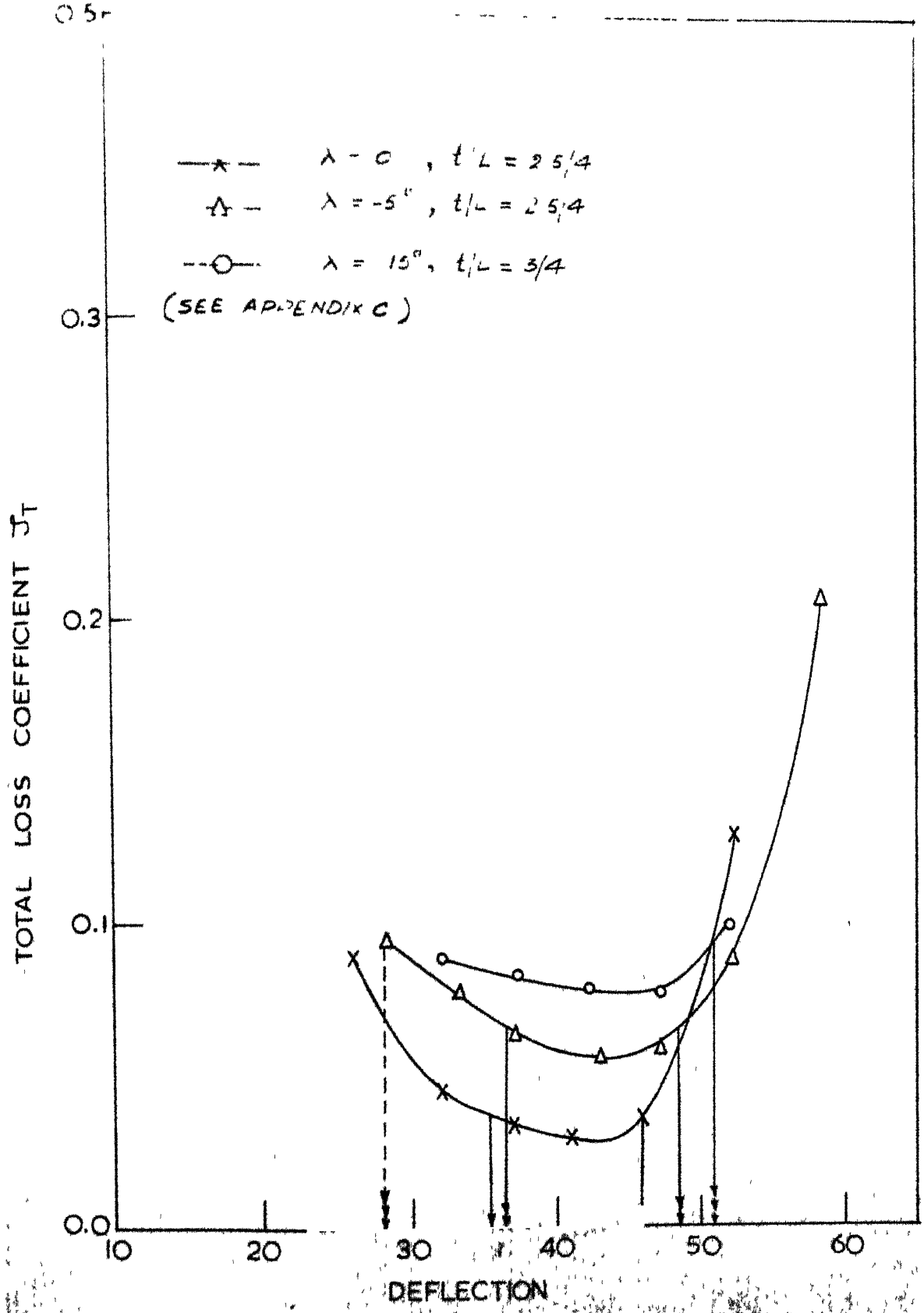

FIG.11- TOTAL LOSS COEFFICIENT VS DEFLECTION

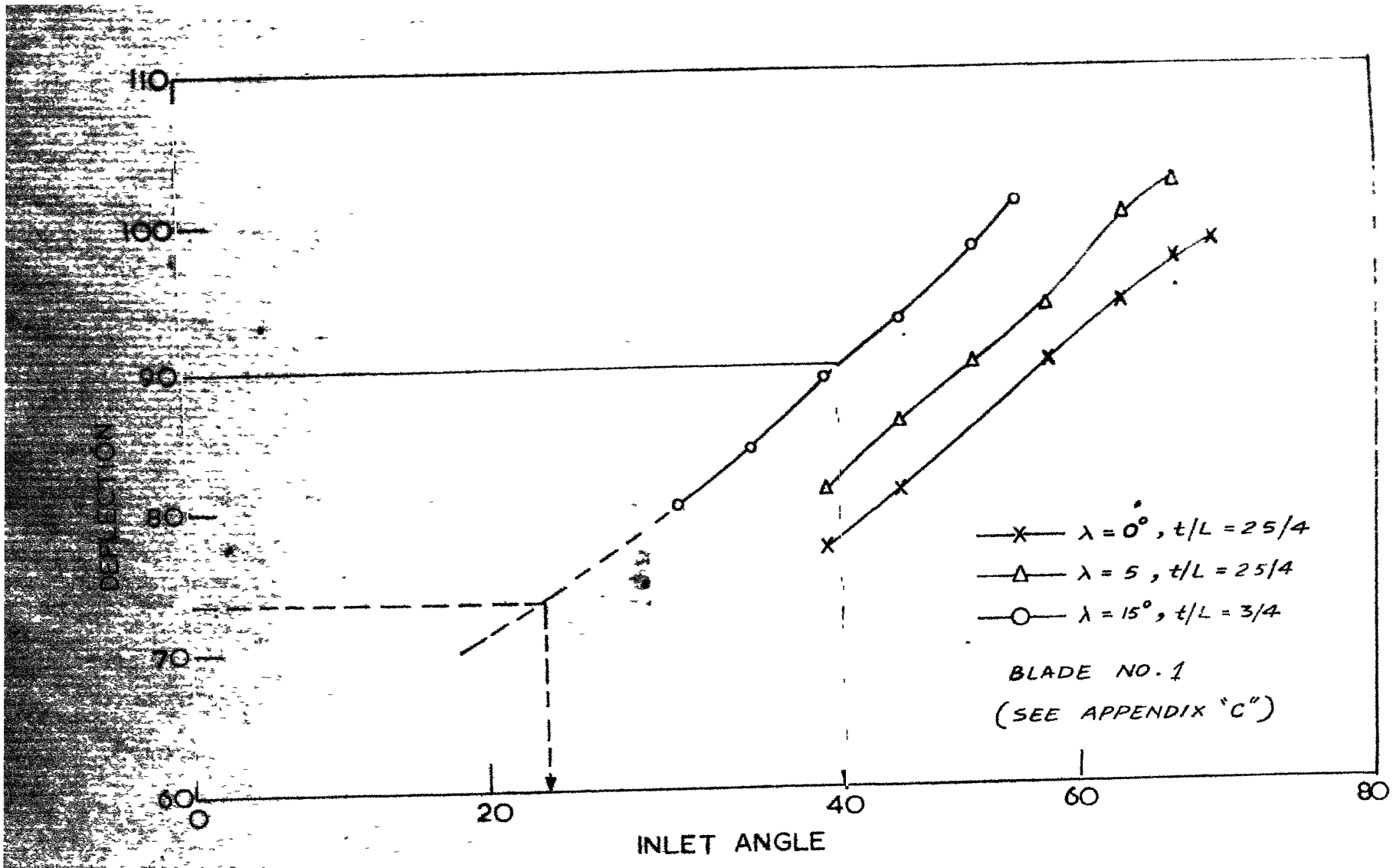

FIG. 12_ DEFLECTION VS INLET ANGLE

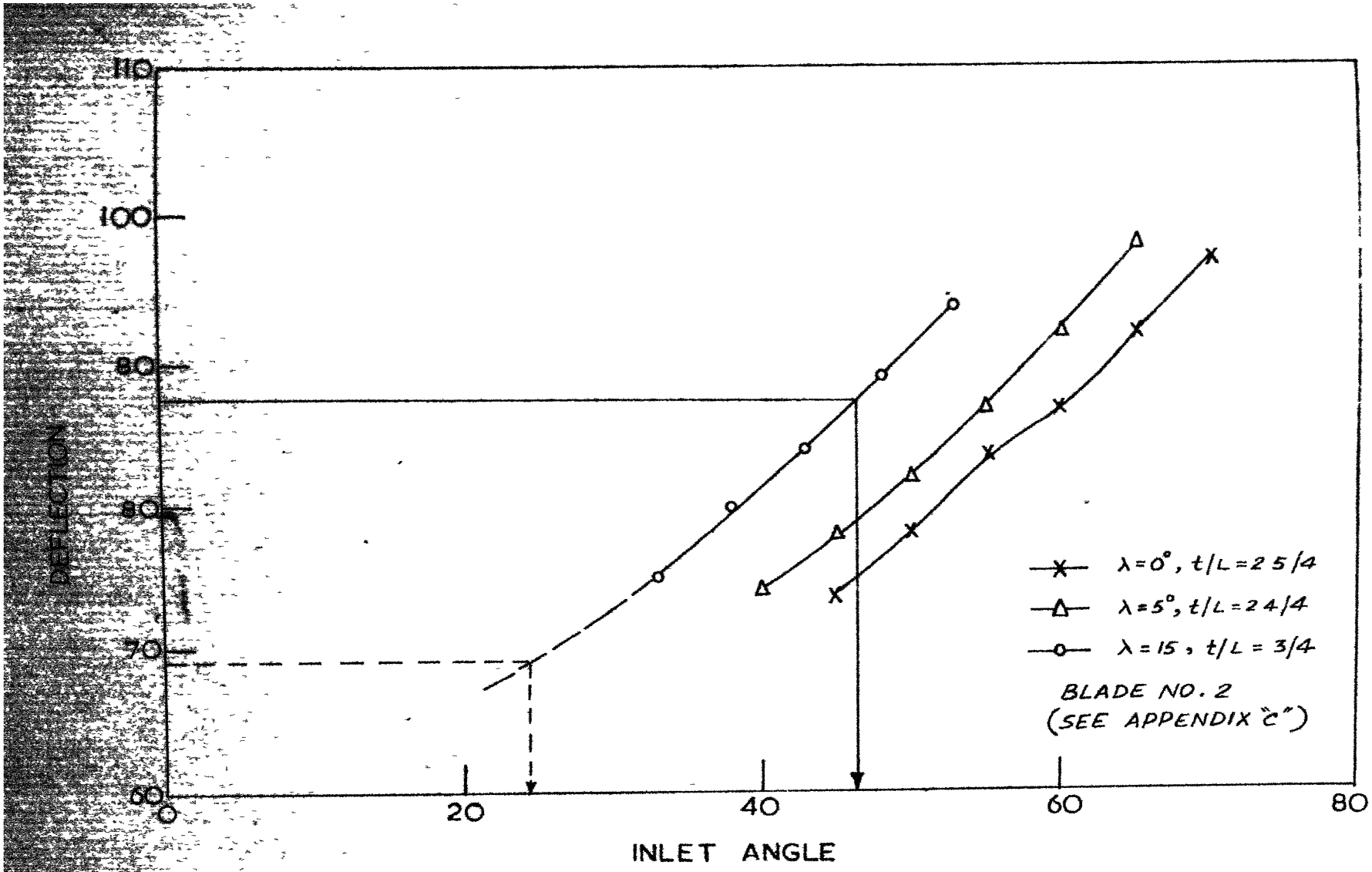

FIG.13_ DEFLECTION VS INLET ANGLE .

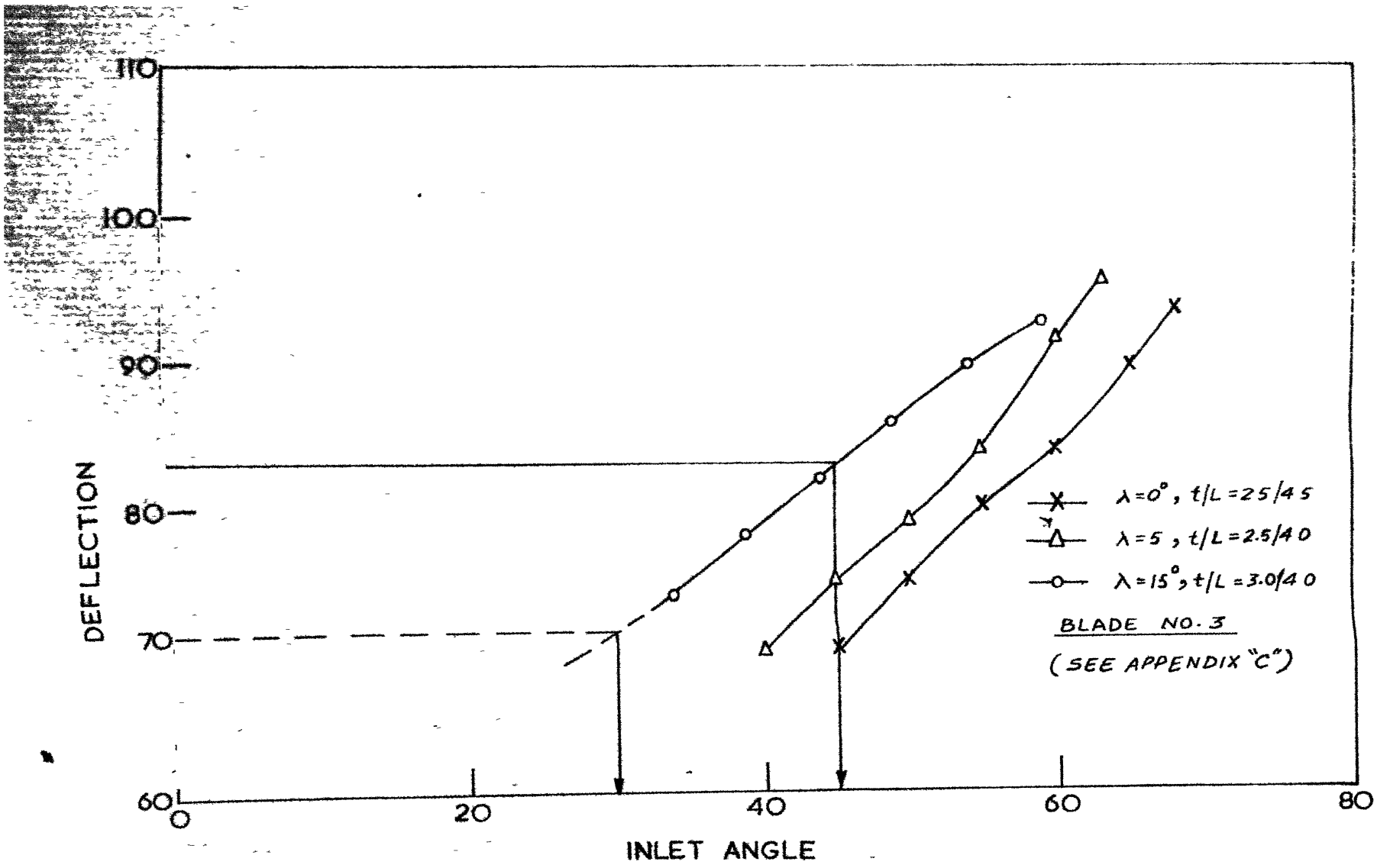

FIG.14_DEFLEFTION VS INLET ANGLE

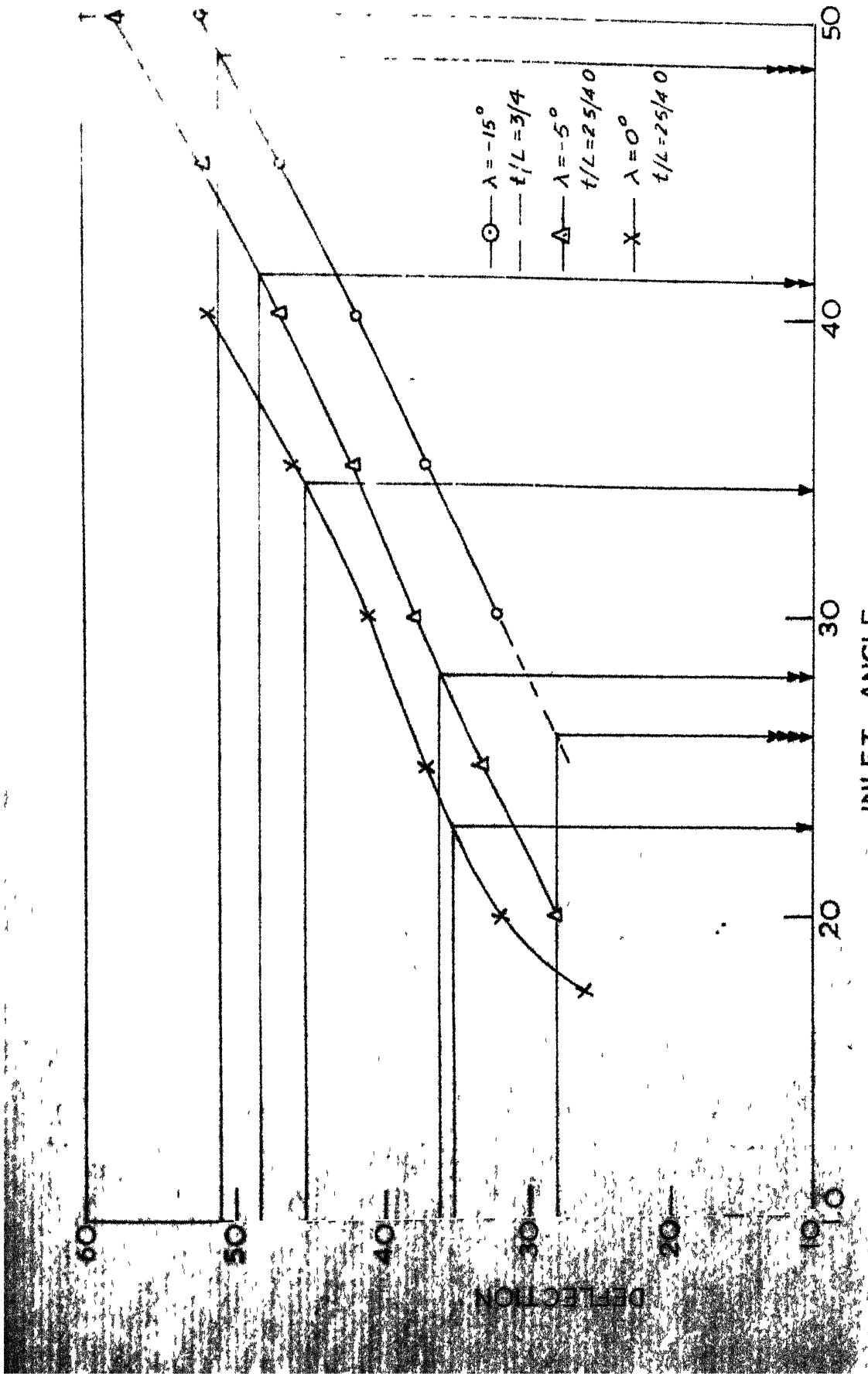

FIG.15_DEFLECTION VS INLET ANGLE BLADE NO_4

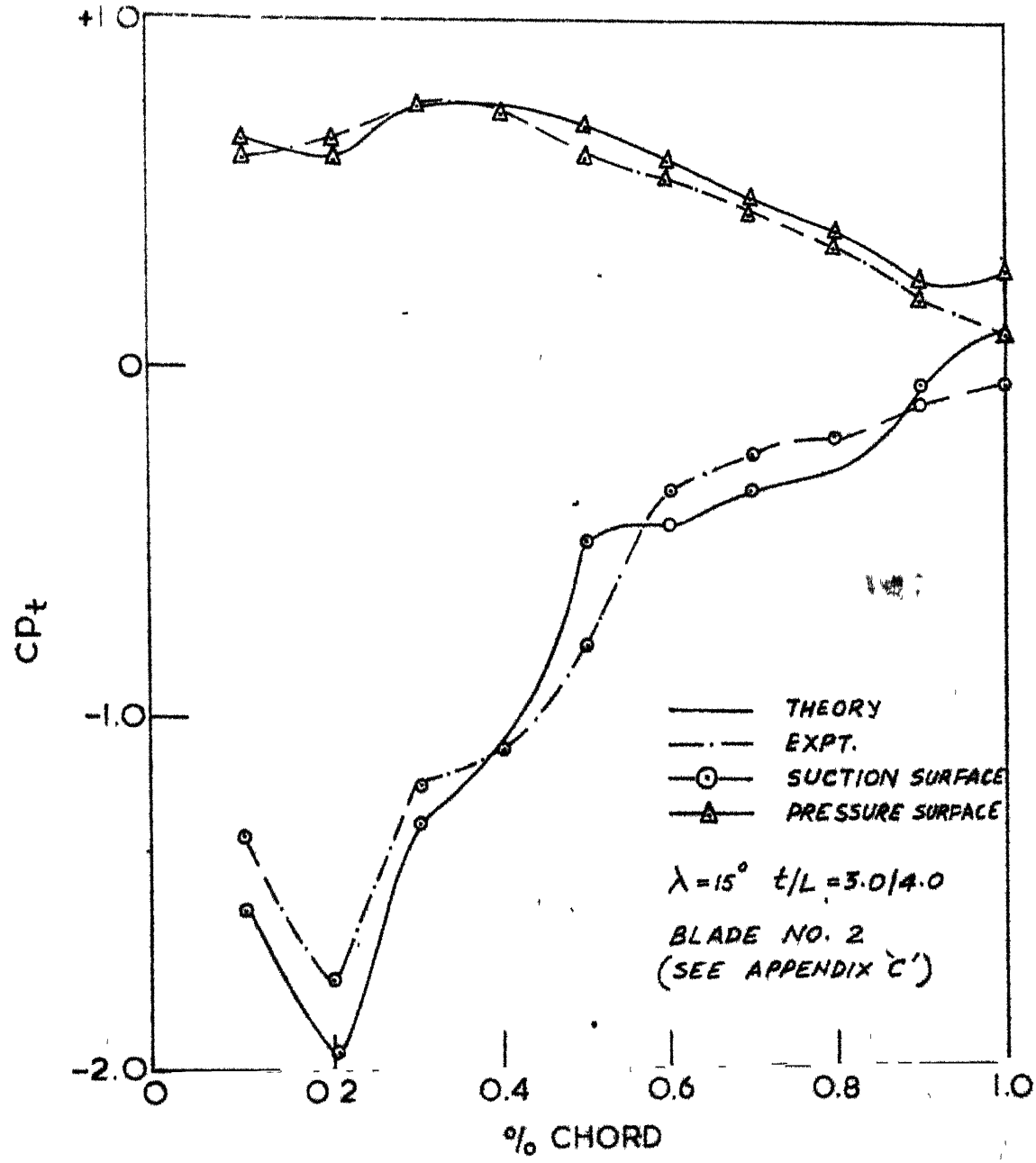

FIG.16_PRESSURE DISTRIBUTION ON A TYPICAL TURBINE BLADE.

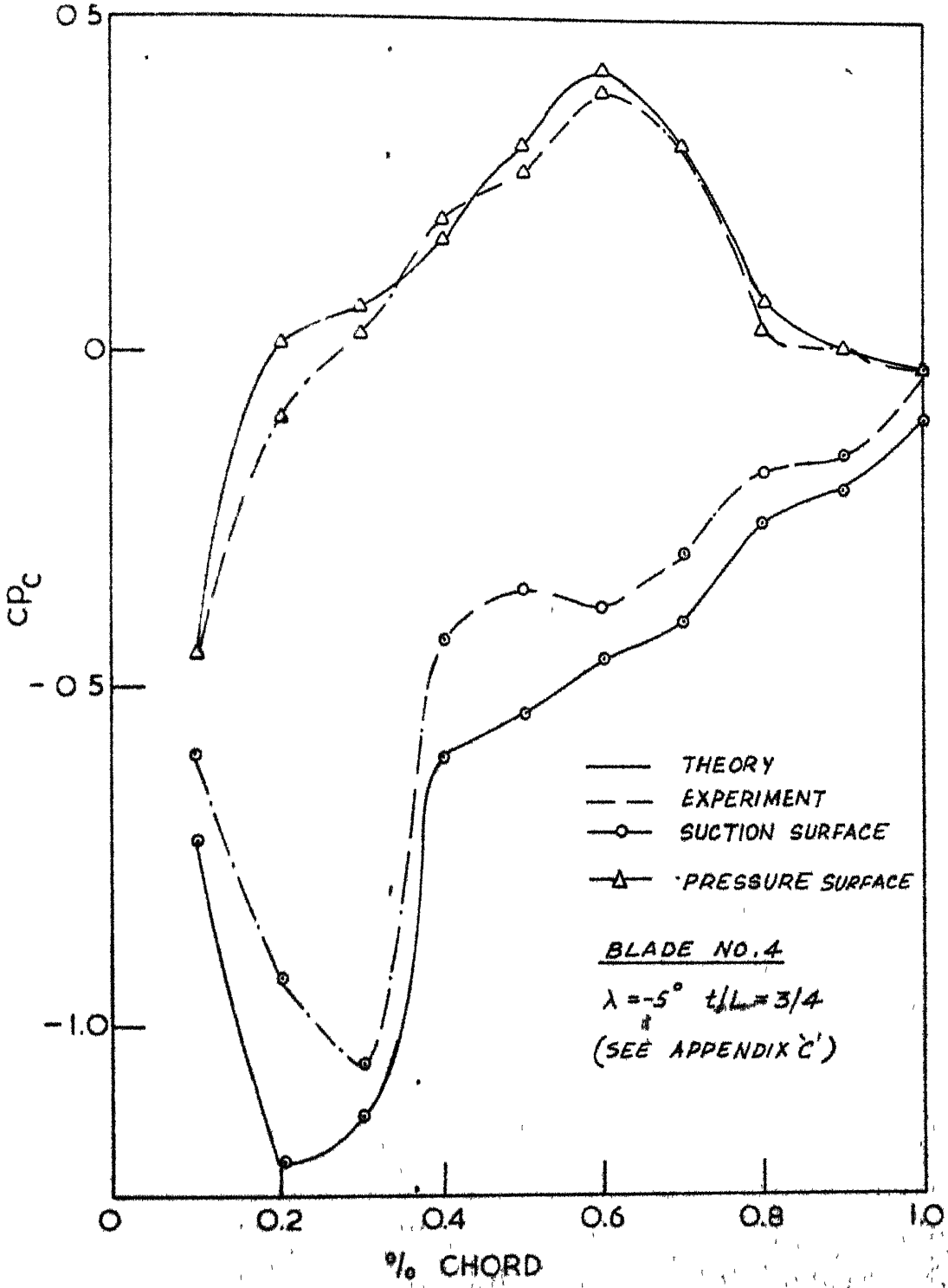

FIG 17_PRESSURE DISTRIBUTION ON TYPICAL COMPRESSOR BLADE

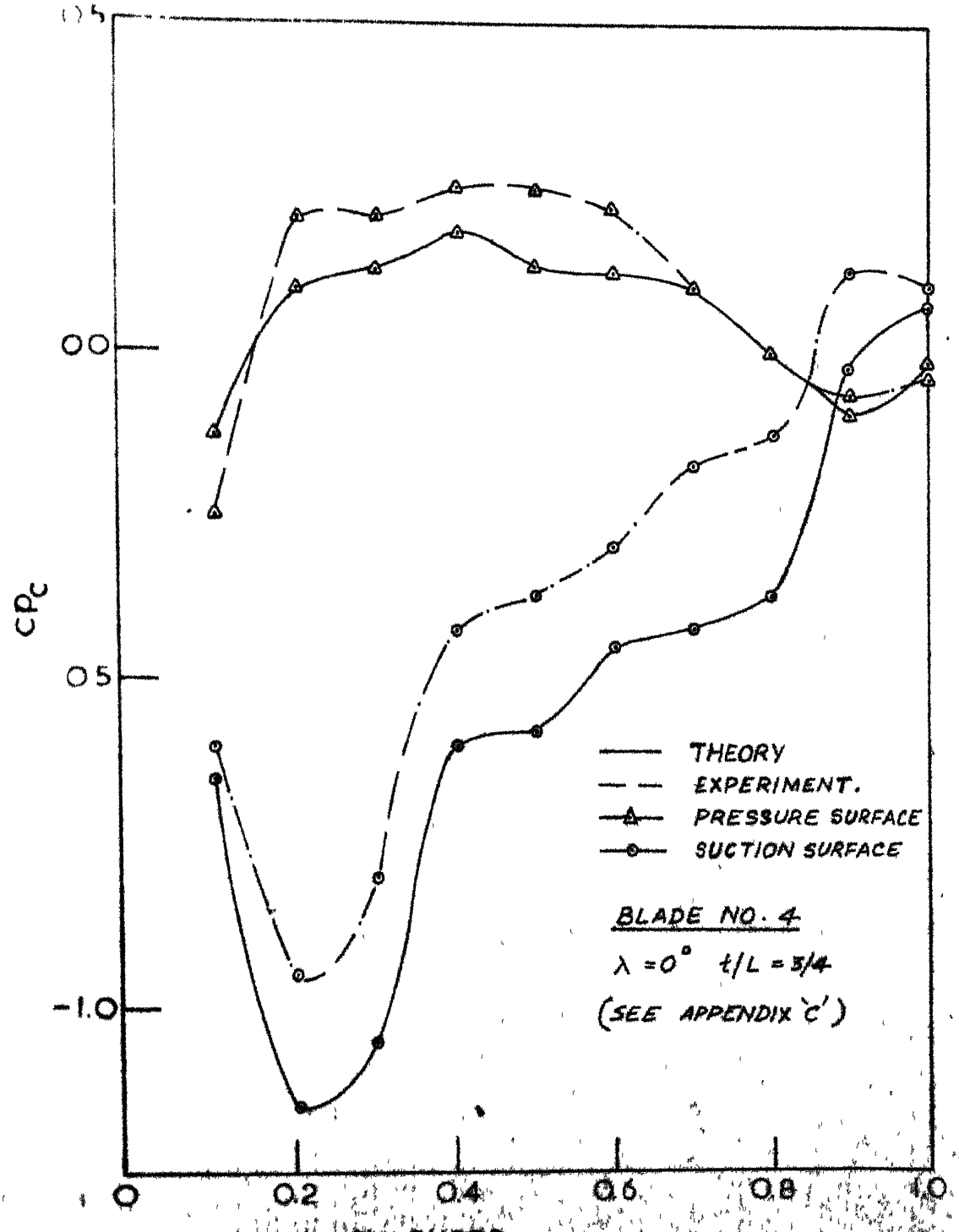

FIG. 18 PRESSURE DISTRIBUTION ON TYPICAL COMPRESSOR BLADE.

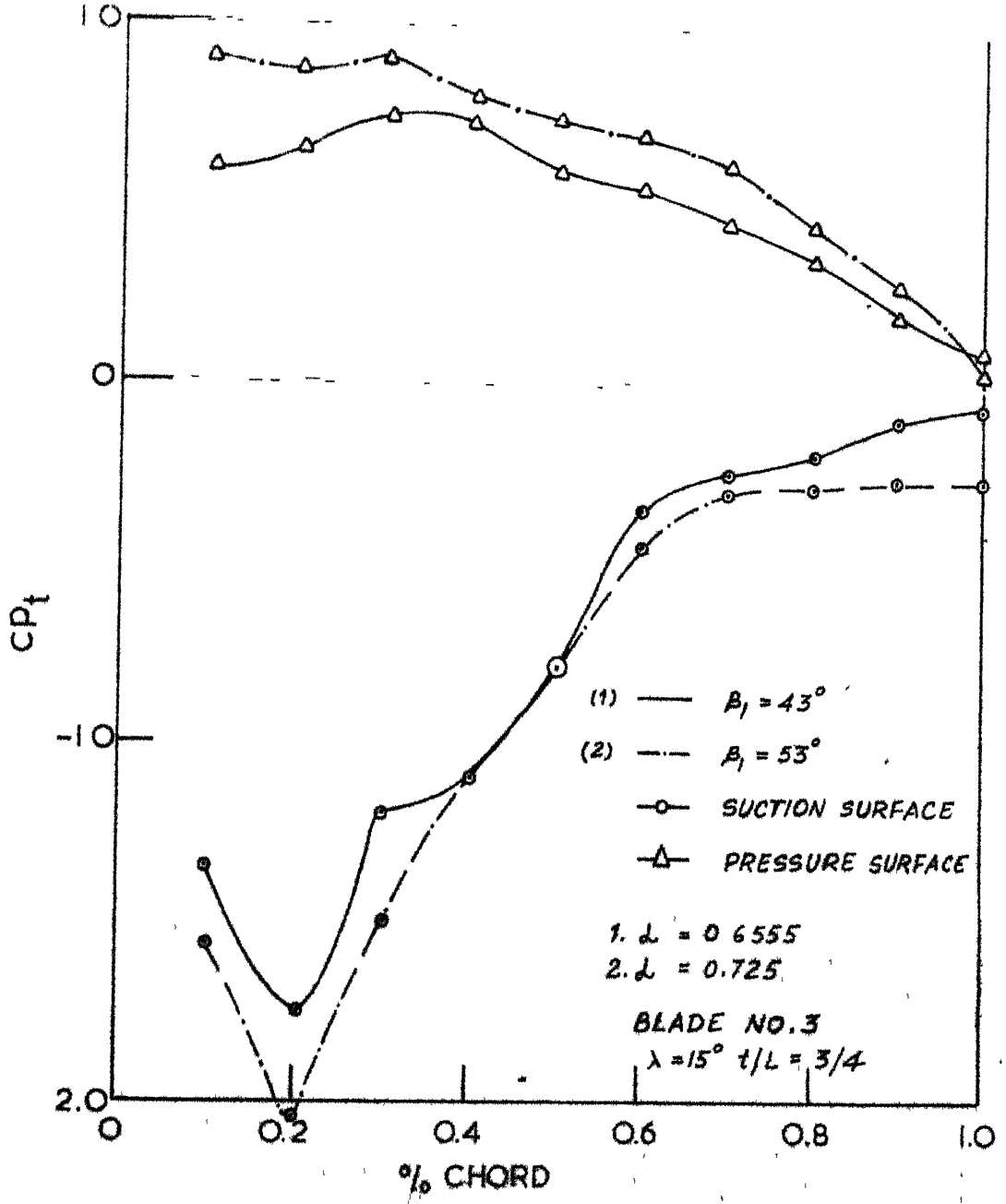

FIG. 19 - STALL EFFECT.

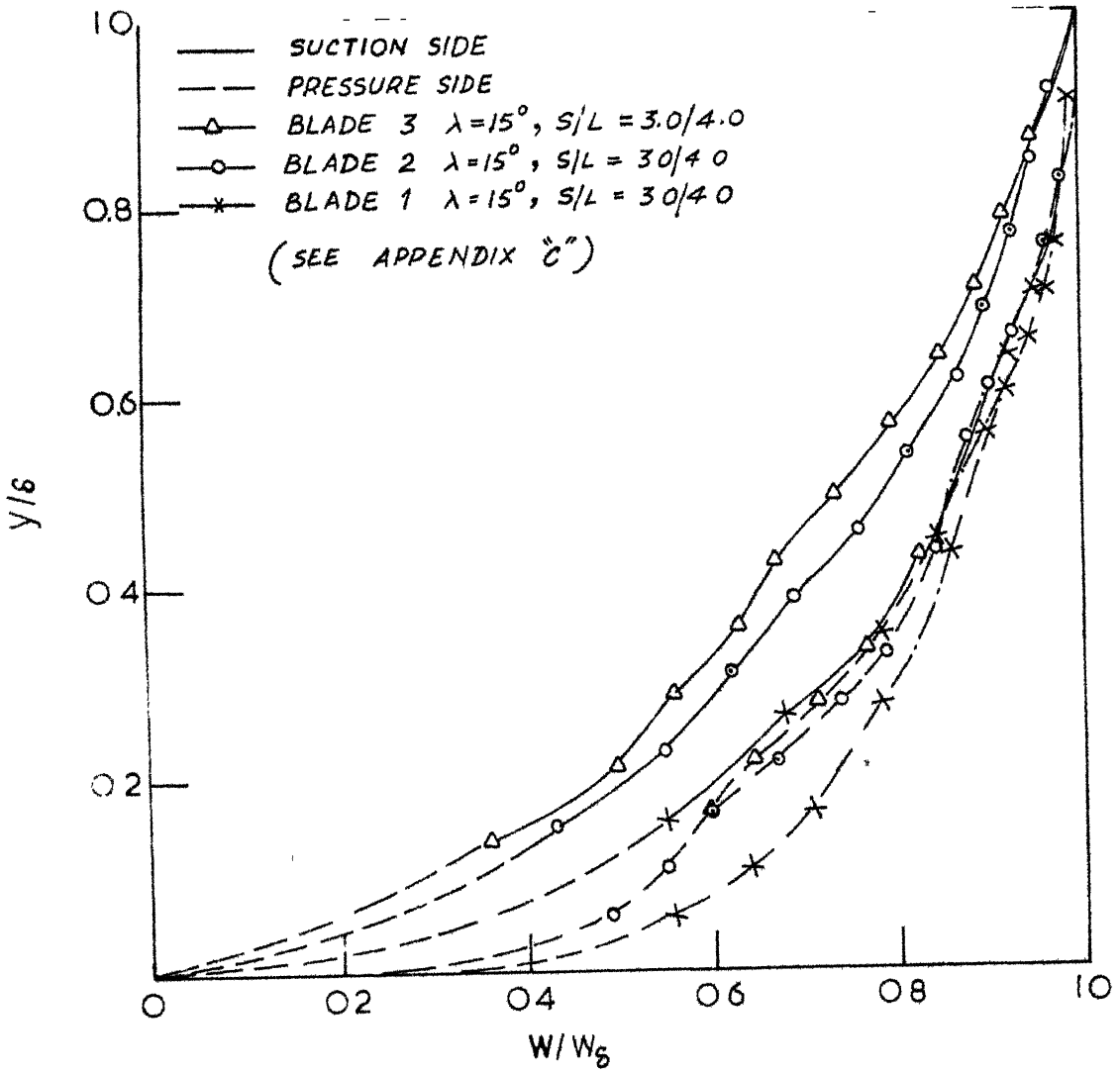

FIG 20 _ BOUNDARY LAYER PROFILES

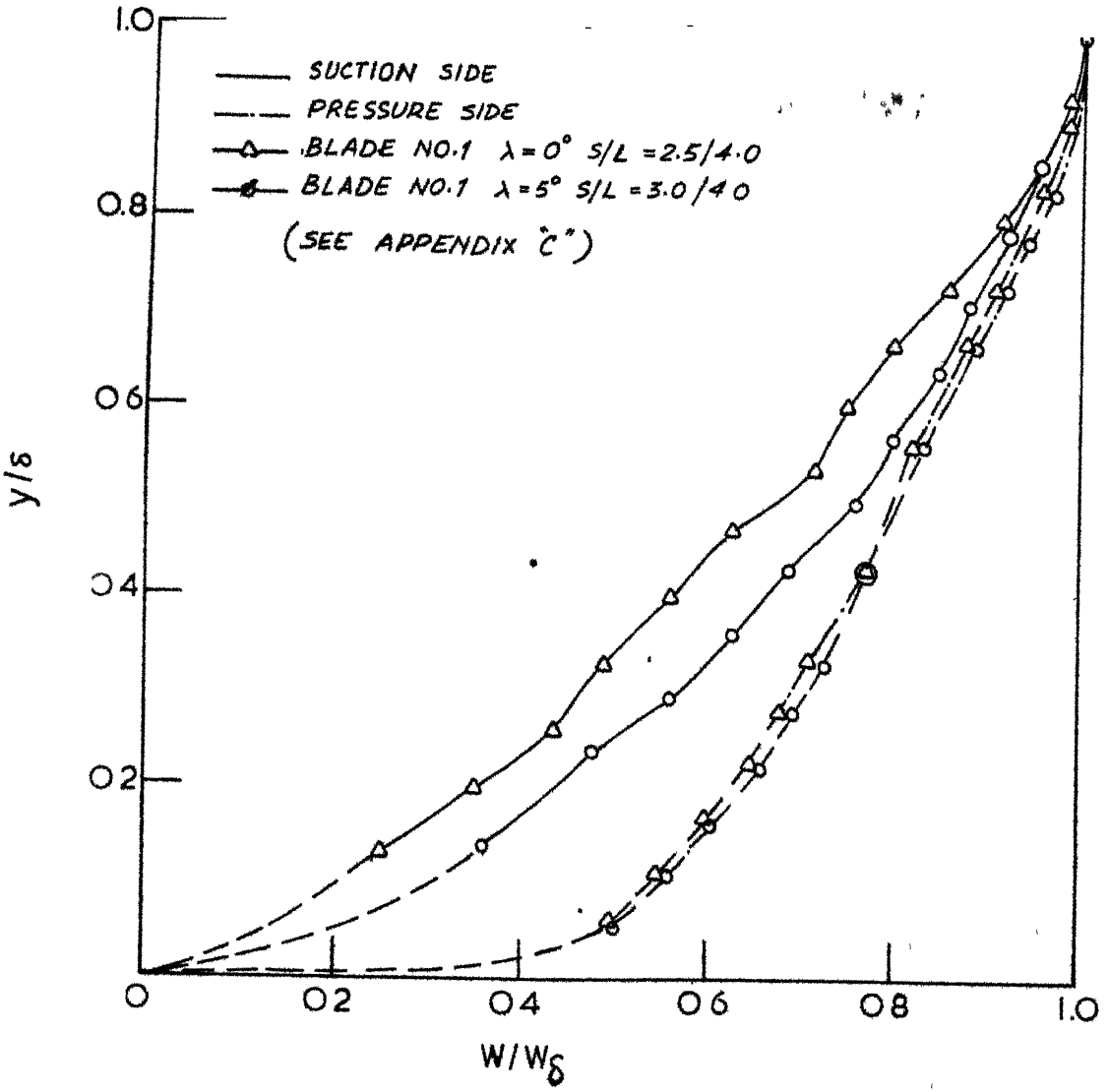

FIG.21 – BOUNDARY LAYER PROFILES

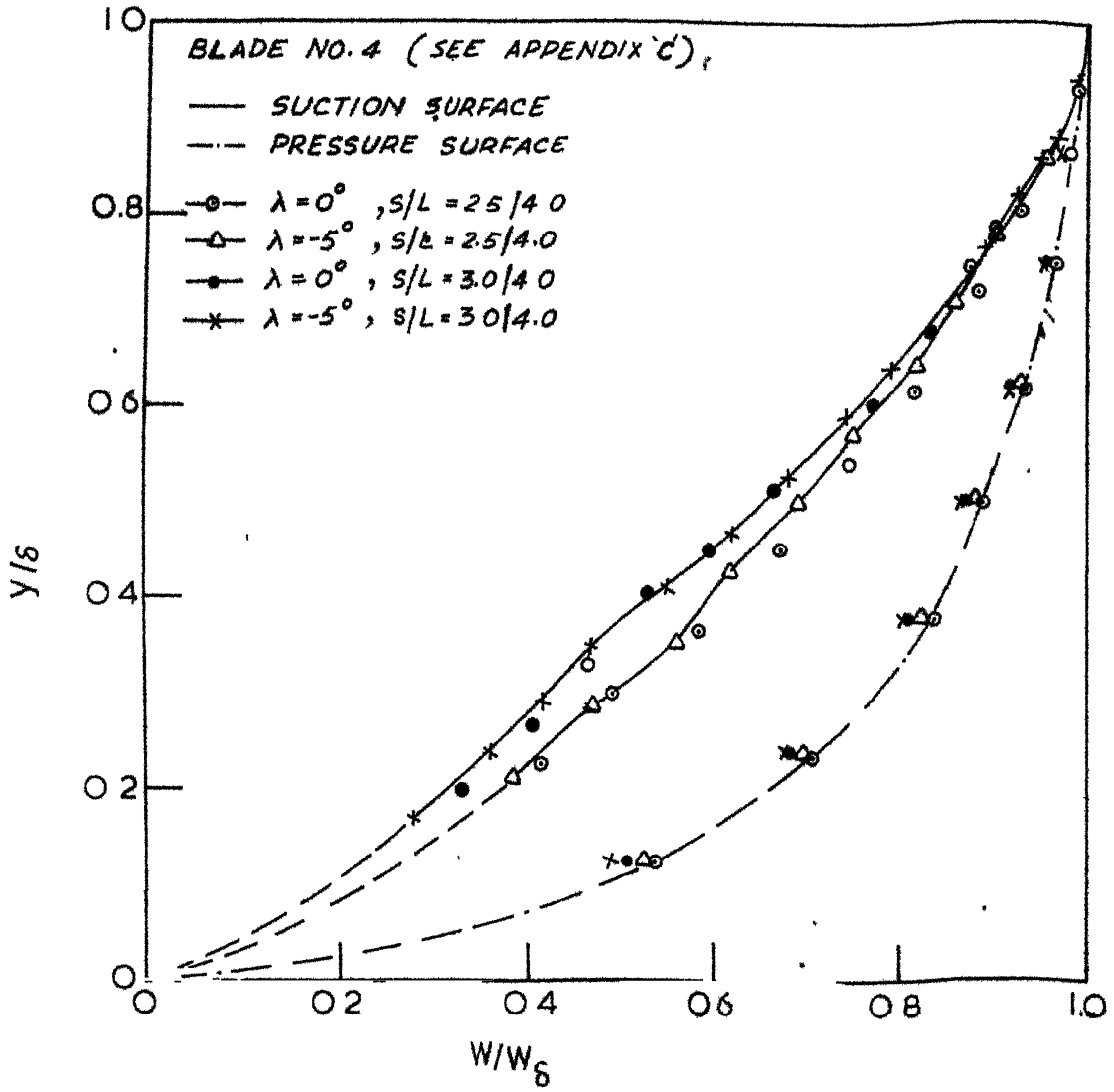

FIG. 22 _ BOUNDARY LAYER PROFILES

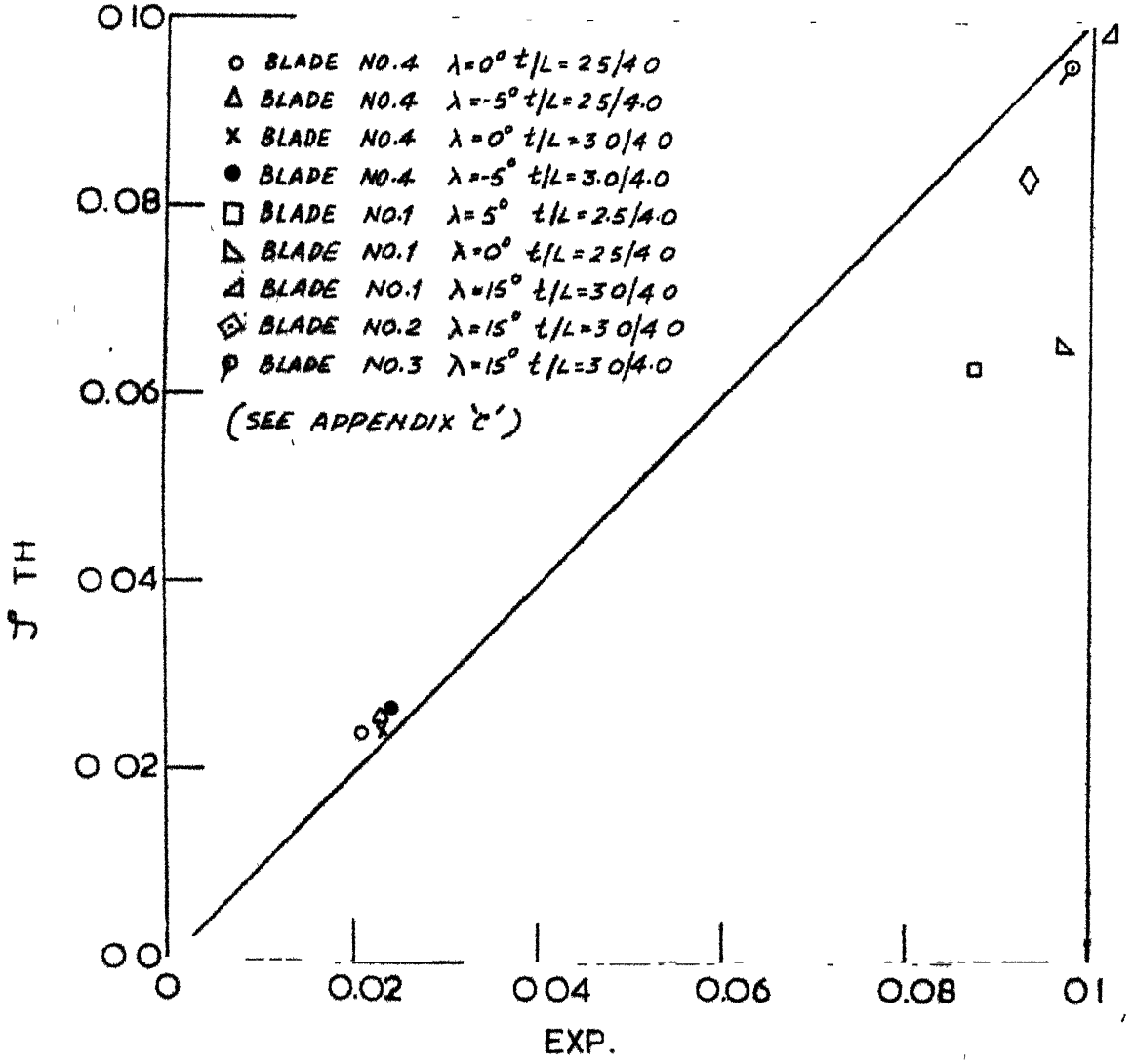

FIG.23_COMPARISION OF EXPERIMENTAL AND THEORETICAL LOSS COEFFICIENTS.

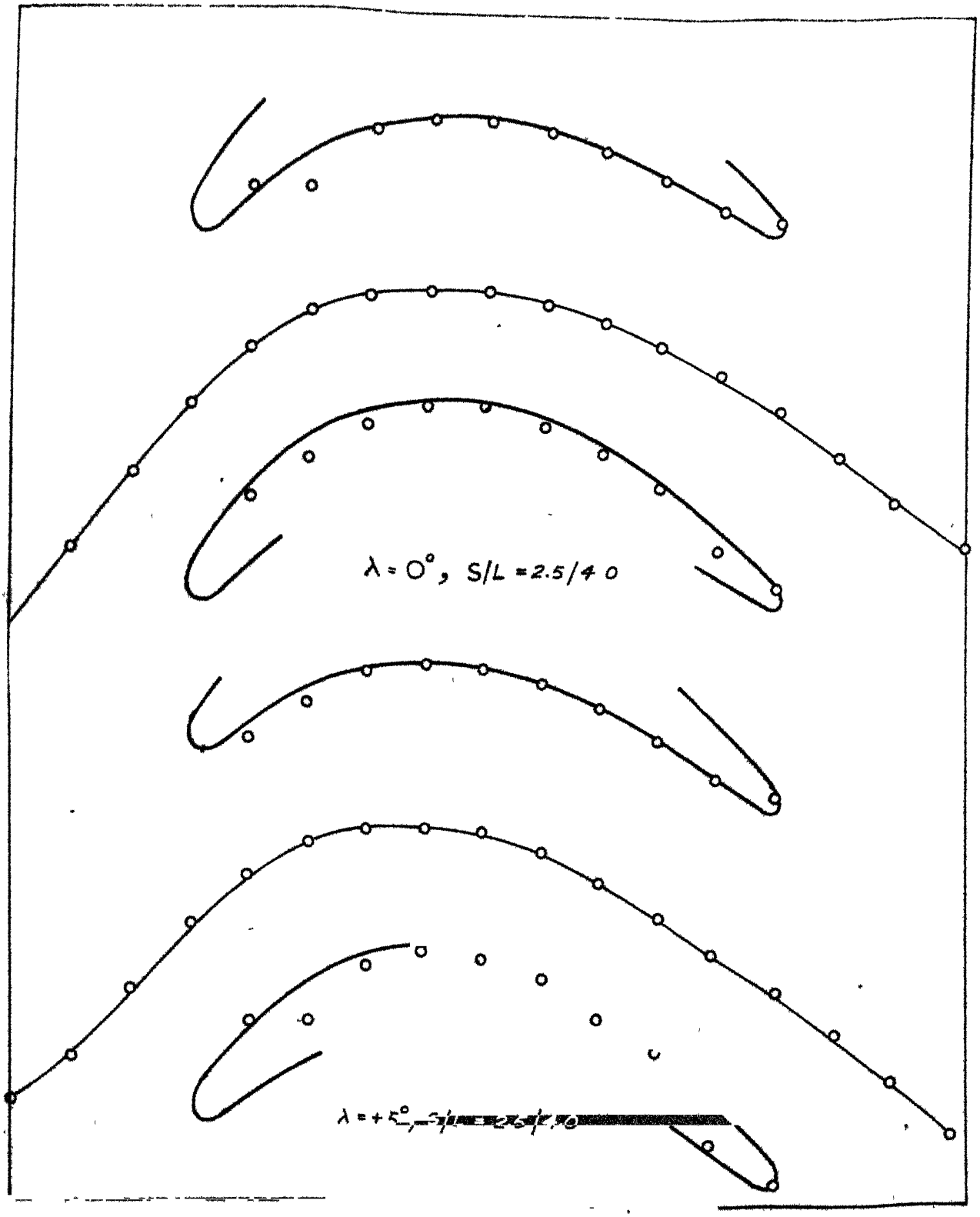

ACTUAL PROFILE

PROFILE POINTS FROM CALCULATIONS

MEAN-STREAM-LINE

FIG 24_ BLADE NO.1

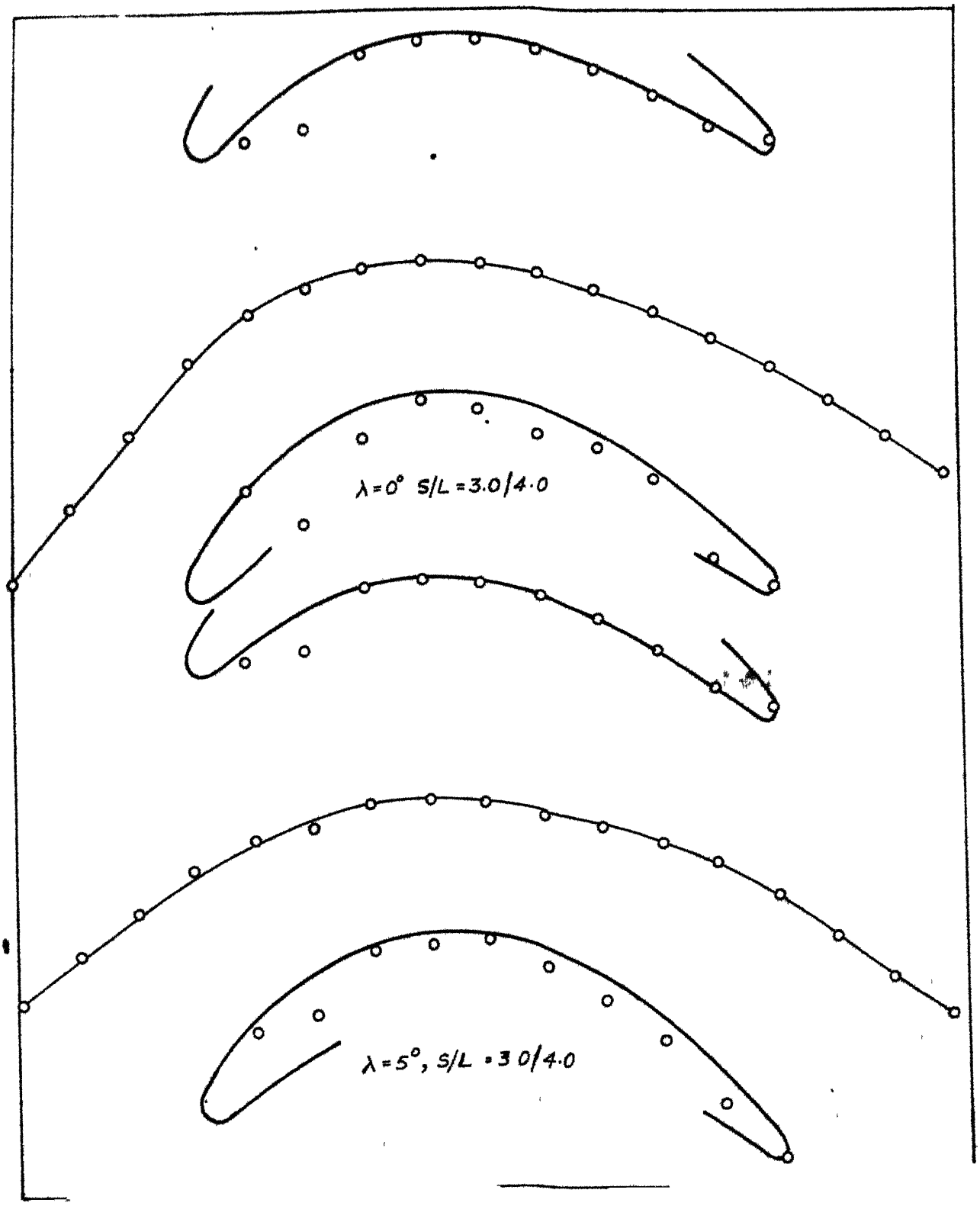

ACTUAL PROFILE

PROFILE POINTS FROM CALCULATIONS

MEAN STREAM-LINE

FIG. 25 - BLADE NO 2

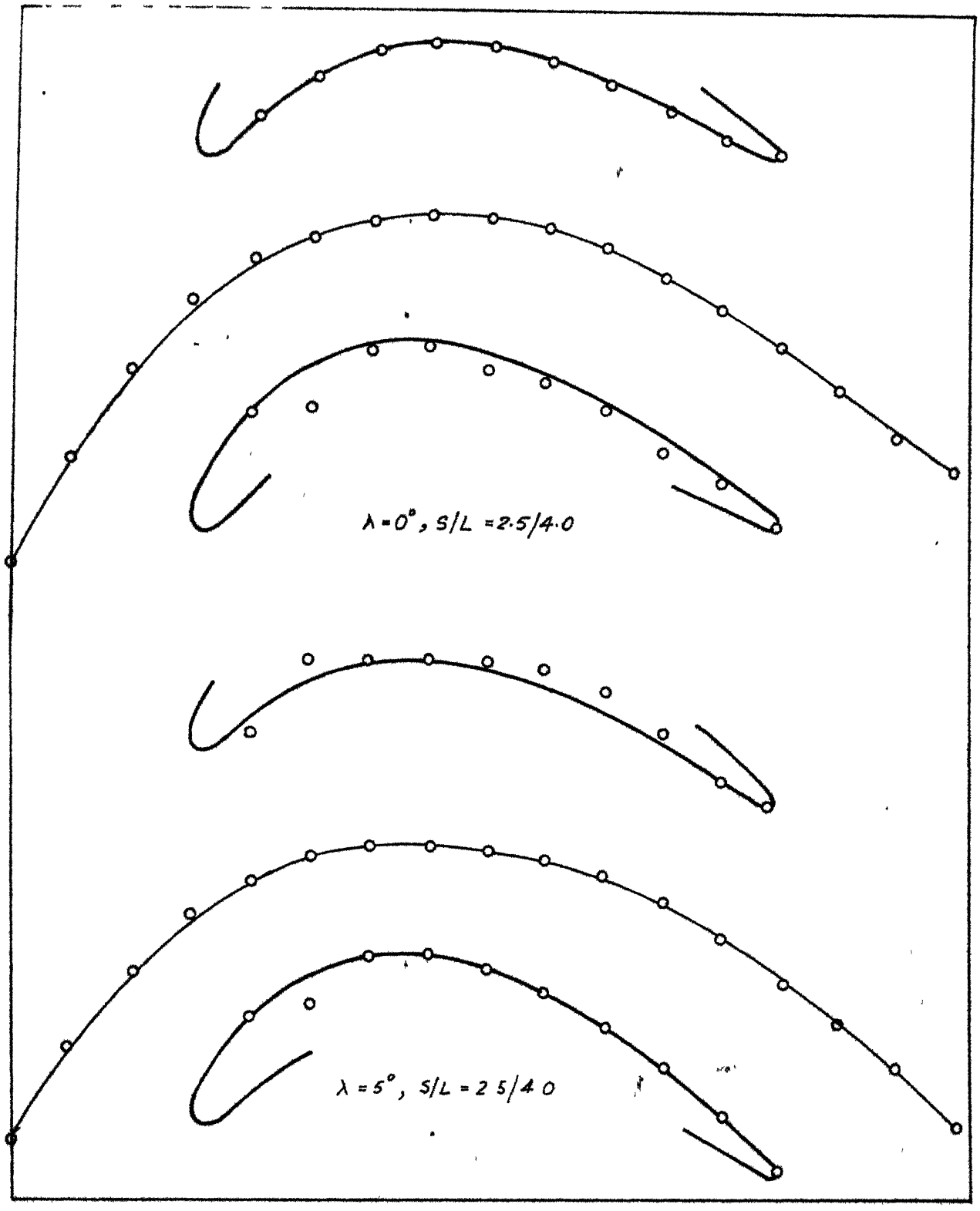

——— ACTUAL PROFILE

ooooo PROFILE POINTS OBTAINED BY CALCULATION

o-o-o-o MEAN - STREAM - LINE

FIG. 26_ BLADE NO. 2

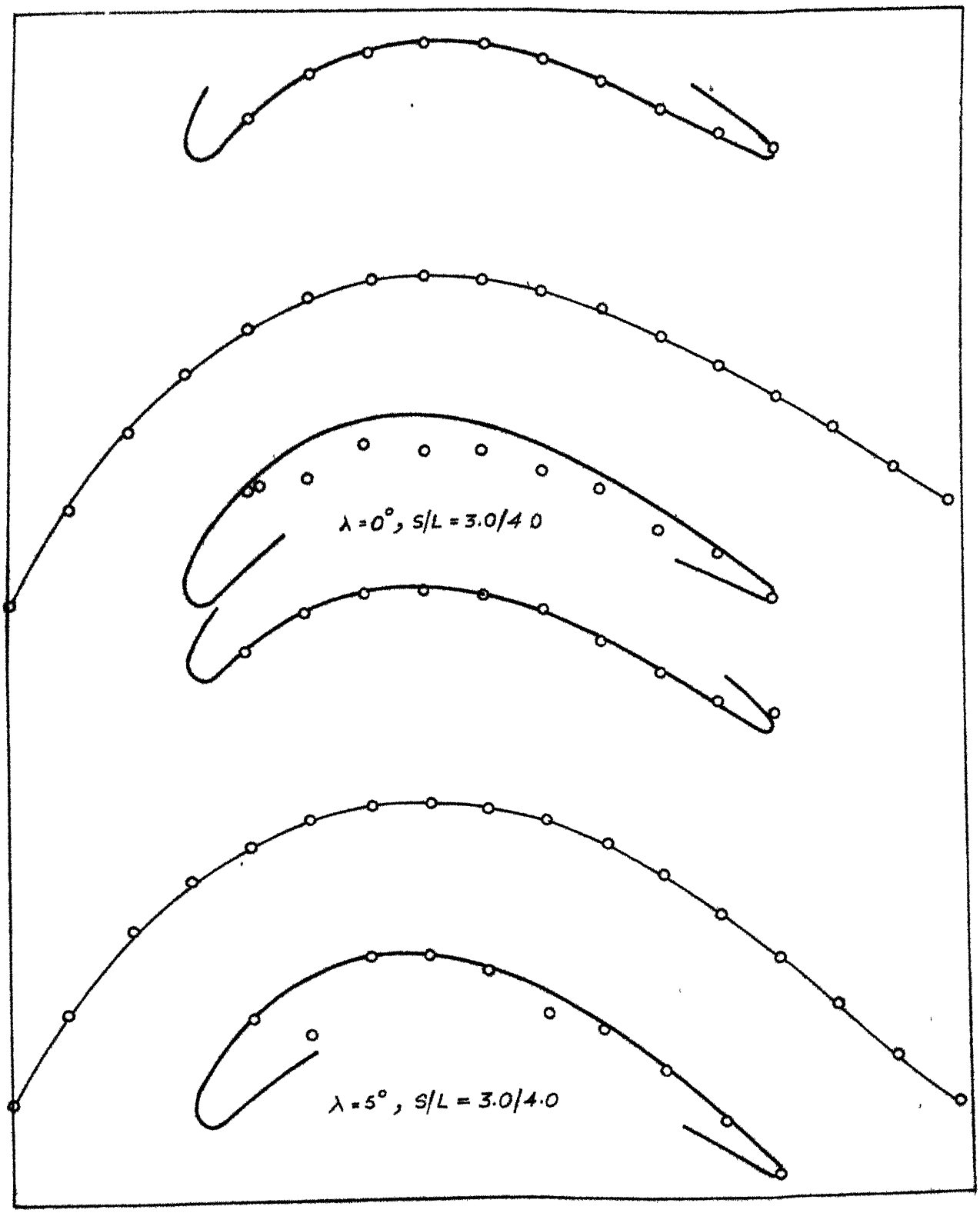

——— ACTUAL PROFILE.

ooooo PROFILE POINTS OBTAINED BY CALCULATIONS.

-o-o-o- MEAN-STREAM-LINE.

FIG. 27_ BLADE NO. 2

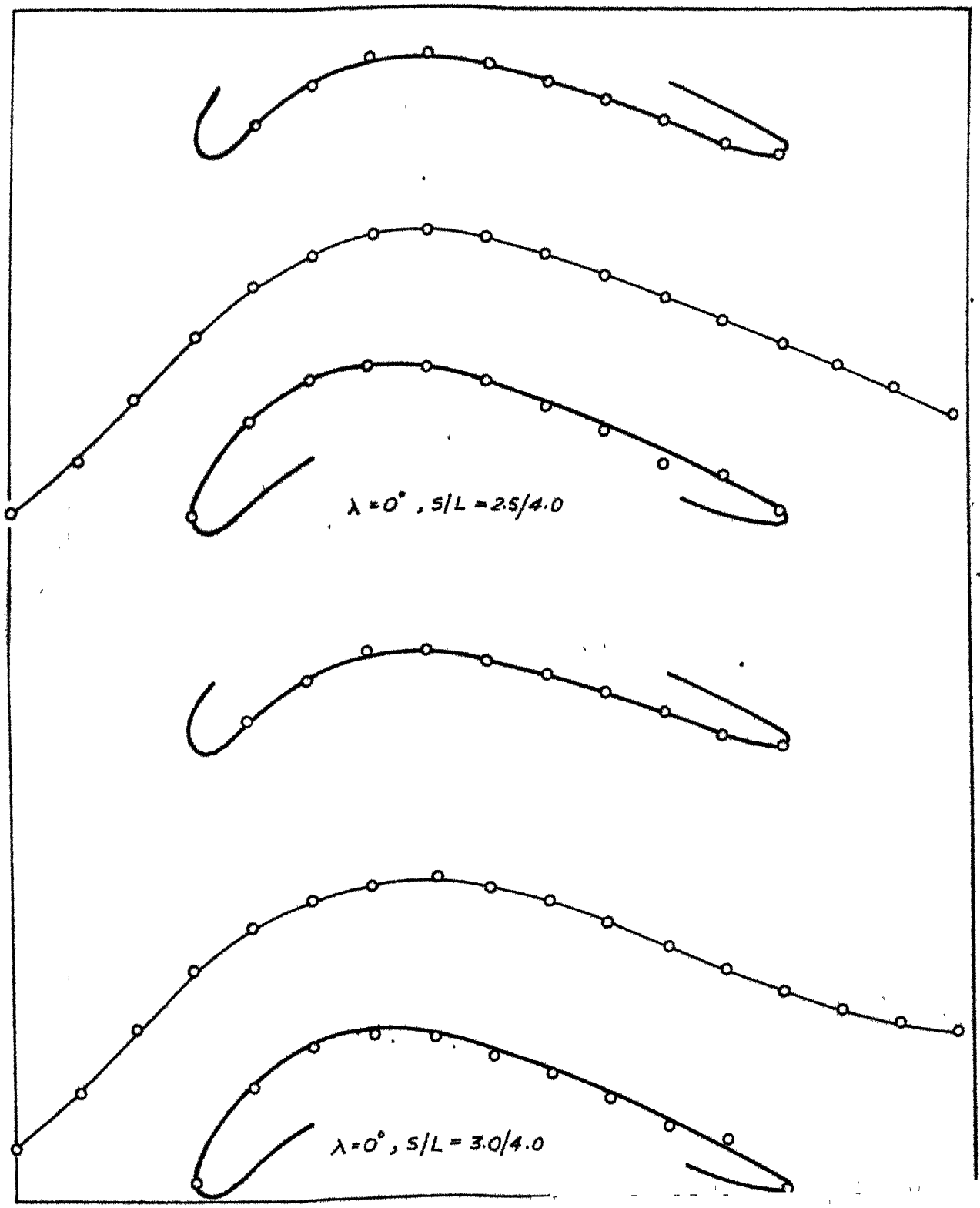

——— ACTUAL PROFILE

ooooo PROFILE POINTS OBTAINED BY CALCULATIONS

-o-o-o- MEAN - STREAM - LINE

FIG. 28 - BLADE NO. 3

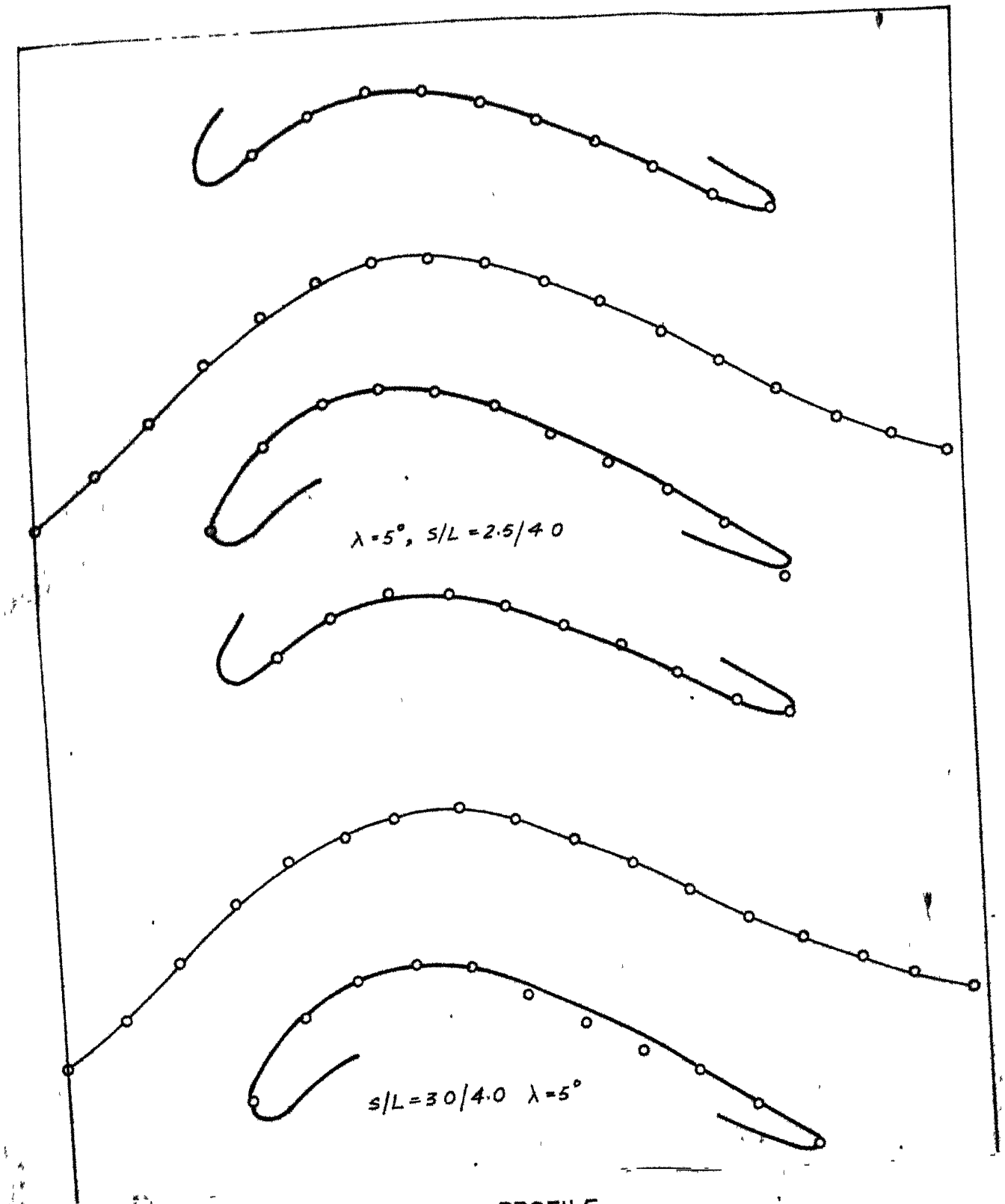

ACTUAL PROFILE.

PROFILE POINTS OBTAINED BY CALCULATION.

MEAN - STREAM - LINE

FIG. 29_ BLADE NO 3

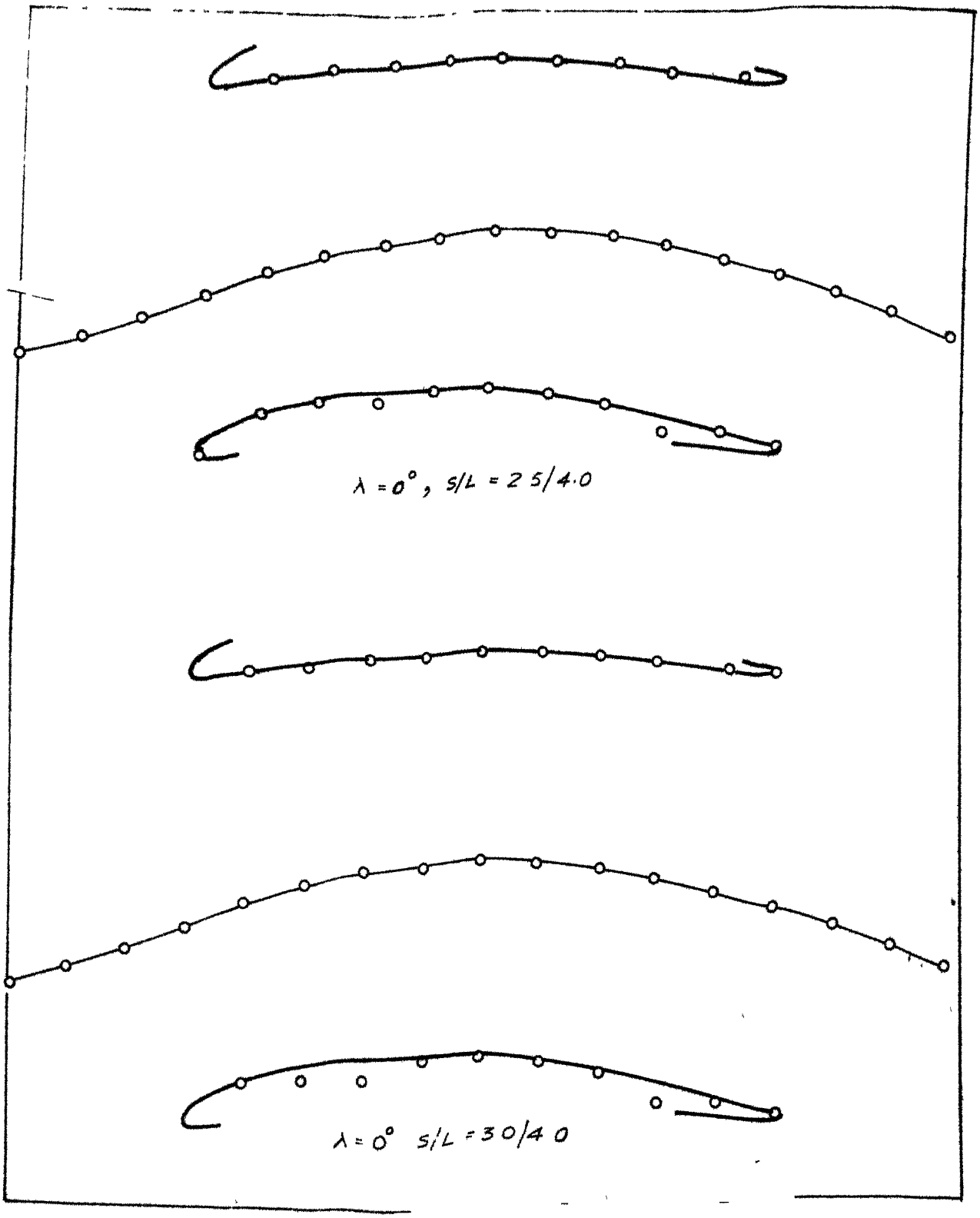

ACTUAL PROFILE

PROFILE POINTS OBTAINED BY CALCULATIONS.

MEAN – STREAM – LINE

FIG 30_ BLADE NO 4

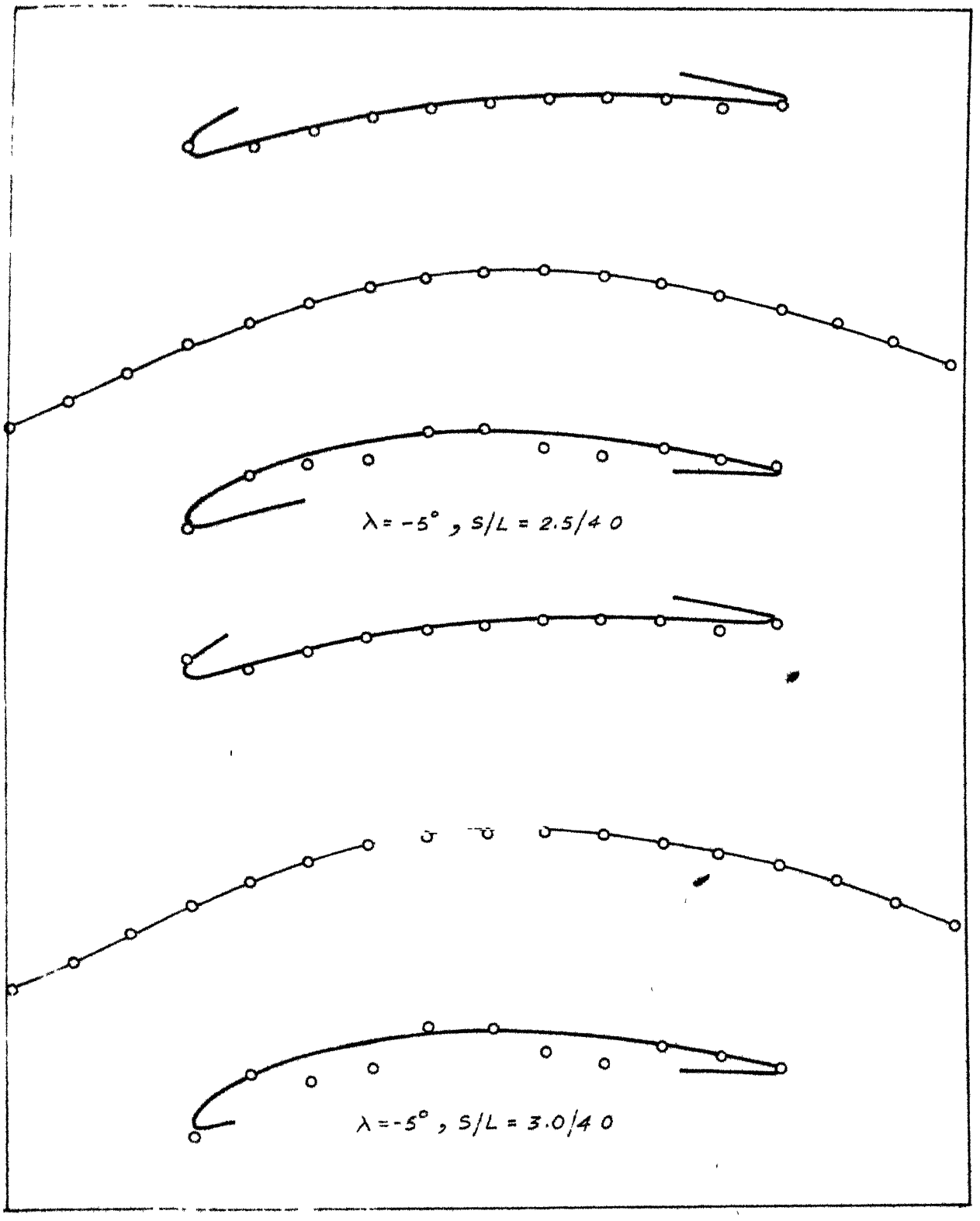

——— ACTUAL PROFILE

ooooo PROFILE POINTS OBTAINED BY CALCULATIONS

oooo-o MEAN STREAM LINE

FIG 31 _ BLADE NO. 4

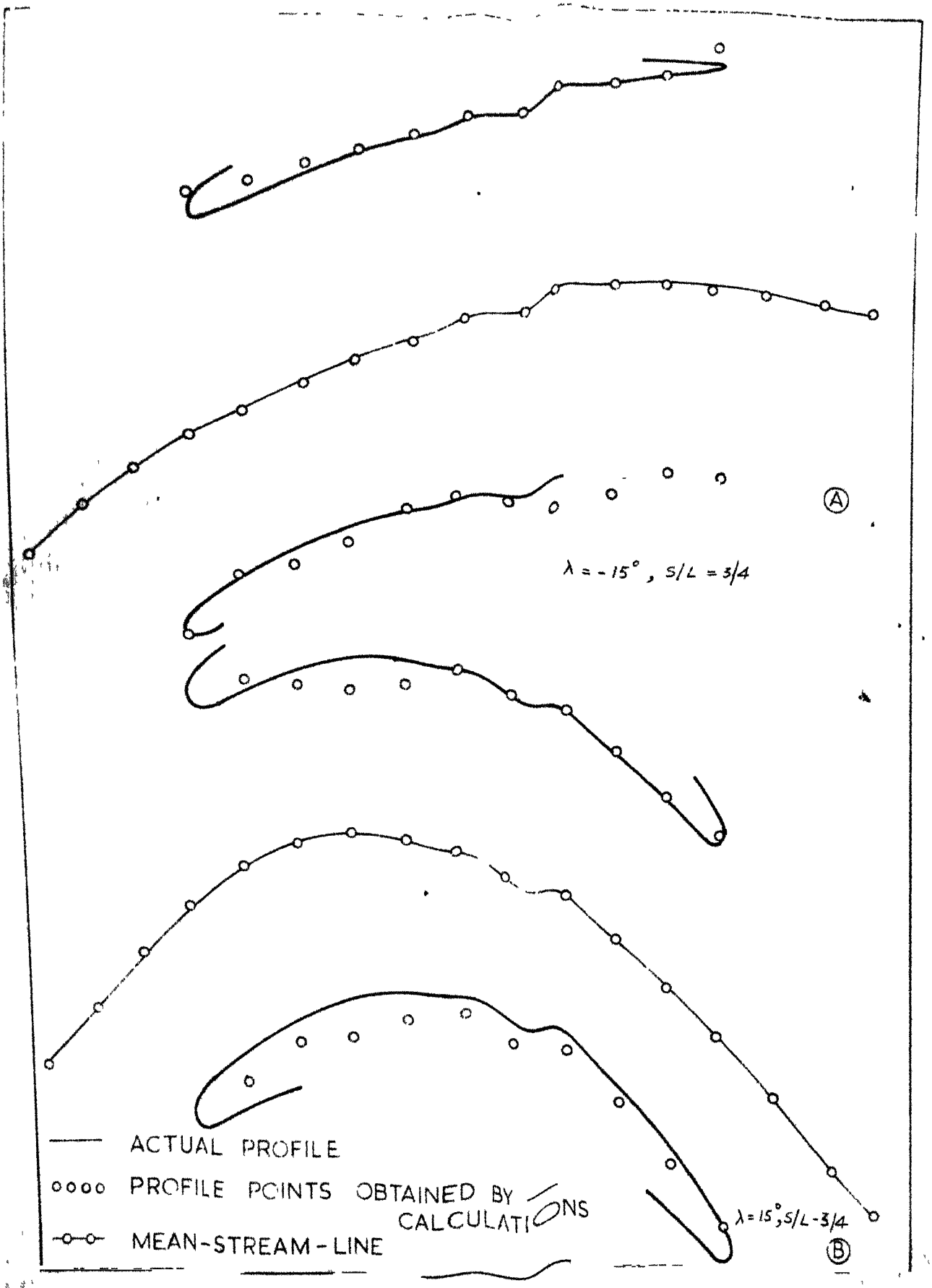

FIG 32 - Ⓐ - BLADE NO 4 Ⓑ BLADE NO 1

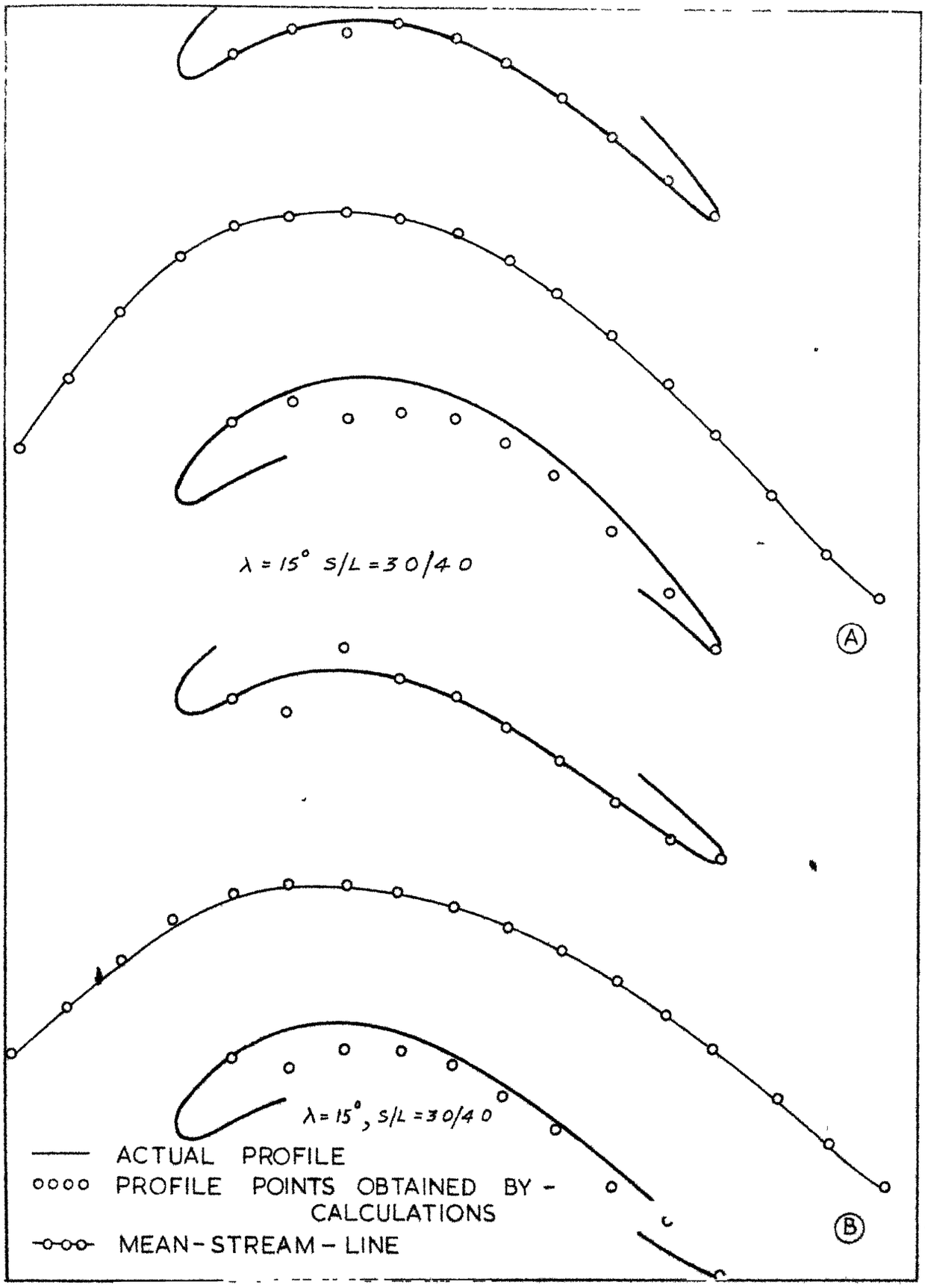

FIG 33_ (A) BLADE NO 2 (B) BLADE NO. 3